Studies of the cosmic ray shadow of the moon and the sun in the KM3NeT/ORCA detector

THESIS

submitted in partial fulfillment of the
requirements for the degree of

BACHELOR OF SCIENCE
in
PHYSICS

Author :	Casper Murris
Student ID :	s184300
Supervisor :	Dorothea Samtleben
2^{nd} corrector :	Tjerk Oosterkamp

Leiden, The Netherlands, June 22, 2020

Studies of the cosmic ray shadow of the moon and the sun in the KM3NeT/ORCA detector

Casper Murris

Huygens-Kamerlingh Onnes Laboratory, Leiden University
P.O. Box 9500, 2300 RA Leiden, The Netherlands

June 22, 2020

Abstract

The research collaboration KM3NeT is currently constructing neutrino telescopes at two sites in the Mediterranean Sea. The pointing accuracy of these two telescopes is of high importance to be able to trace detected neutrinos back to their cosmic sources. Pointing can be cross checked with the cosmic ray shadow of the moon respectively the sun. In this research first the effects of mispointing of the KM3NeT/ORCA detector on the 2D map of the moon were evaluated. It is shown how various mispointing does in fact distort the 2D-map of a celestial object. Secondly the first six months of data with 4 lines of the KM3NeT/ORCA detector were used to investigate the cosmic ray shadow from both the sun and the moon. Extrapolated simulations for a year show that the statistics are currently not sufficient for a significant deficit of particles in the neighbourhood of the moon and the sun. In the analysis of the ORCA4 data the background of the moon and sun signal was evaluated using fake sources, following the path of the moon and with a given time delay. The background showed significant differences between different fake sources and also could be shown to behave differently for the moon and the sun. Further research is needed to investigate the discovered features and be able to recover the signal from the moon and sun shadows.

Contents

Chapter 1

Introduction

The initial aim of this research is to determine whether it is possible to detect a significant cosmic ray shadow of the moon. This cosmic shadow ray is caused by the moon blocking cosmic particles. This project also aims to lay an initial foundation for future investigation of research on cosmic ray shadow detection.

1.1 KM3NeT

The research is conducted in collaboration with the KM3NeT group at Nikhef in Amsterdam. KM3NeT is a research collaboration which is currently building next a generation neutrino telescope at the bottom of the Mediterranean Sea. Once finished, the detectors have a volume of several cubic kilometers, hence the abbreviation KM3NeT: **km^3 Ne**utrino **T**elescope.

The neutrino telescope will consist of several building blocks, which are 3D arrays of highly sensitive optical detectors. Currently there are two of these detectors under construction: ARCA (Astroparticle Research with Cosmics in the Abyss) and ORCA (Oscillation Research with Cosmics in the Abyss), located respectively off the Italian and French coast[1].

The two building blocks are not used for the same scientific goals. The ORCA detector is used to study the mass hierarchy of neutrinos. The objective for ARCA is the detection of high energy neutrinos coming from the cosmos[2]. For example the high-energy neutrino production in quasars[3]. A quasar is visible in the electromagnetic spectrum because it emits light. But neutrinos tell something about the weak interactions in this object. In this research I will evaluate the data from ORCA. But the methods described in this thesis are reusable for other detectors like ARCA.

1.2 Detection method

Detecting neutrinos is a difficult task and can't be done with normal telescopes. Besides the fact that neutrinos are chargeless, they are also nearly massless. A neutrino is also a lepton. Having these attributes cause a neutrino to only interact with the weak force*[4]. This is why neutrinos do not interact a lot with other matter. Cosmic neutrinos can reach the Earth, while other cosmic particles may not. These traits are also the reason why neutrinos are difficult to detect. Hence we rely on the few neutrinos that do interact with other matter.

The weak interaction of neutrinos with nucleons creating charged particles are useful for the detection. When a charged particle is created, it can get a boost from the initial momentum of the neutrino. The neutrino could boost the charged particle close to the speed of light. As this charged particle enters a medium, its velocity could be larger than the speed of light in that medium: $v > c/n$, where n is the refractive index of water in this case. If this happens, the charged particle will polarise the medium and induce so-called Cherenkov radiation. This electromagnetic radiation will traverse as a cone. Where the angle of the cone with respect of the movement of the particle is given as $\cos\theta = \frac{c}{nv}$. This Cherenkov radiation can be detected the sensitive photo detectors in the ORCA and ARCA detectors[2].

Atmospheric muons are also measured by the ORCA and ARCA detectors. These muons are created in the atmosphere by an interaction of cosmic rays, consisting mainly of protons, with the air in the atmosphere. They collide mostly with oxygen and nitrogen. With these collisions they create pions and kaons which in turn decay to muons and neutrinos. Muons and neutrinos are the only particles that are able to penetrate to the depths of the detector[5].

Once completed, a building block consists of 115 strings, or Detector Units (DUs). Every string contains 18 evenly spaced out glass spheres, or Digital Optical Modules (DOMs). These DOMs house 31 "cameras" called PhotoMultiplier Tubes (PMT). These PMTs can detect single photons. And thus these PMTs are the ones that detect the Cherenkov radiation. All the DOMs inside a DU are connected with a power input and a data output. In the ORCA detector the DOMs have a spacing of about 9 meters. The DUs have a horizontal displacement of about 20 meters to their nearest neighbour. Anchored to the ocean floor, they are connected with a network

*Neutrinos also interact with the gravitational force, but the small mass causes it to be negligible.

of cables to shore[2].

A detector is measuring all the time for Cherenkov radiation. Periods of measurements are called runs. These runs do not have fixed length since different runs have different purposes, for example physics runs or calibration runs. Not all radiation gets registered. Once a signal on a PMT hits a threshold of 0.3 photo-electrons, it will be registered as a hit. A hit has two variables, the time when the threshold was met and the total time the signal was above the threshold. The latter is also called the Time-Over-Threshold (ToT). The threshold can be seen as a zero-level filter on the data. Therefore we call this L0 hits. These L0 hits are all send to shore, where the data processing proceeds.

With different algorithms the first onshore data filter gives L1 hits. This filter checks if another PMT on the same DOM also registered a L0 hit in a certain time interval. The higher the multiplicity of L0 hits on a DOM, the likelier the original light source originates from a physical particle. [2].
With different L1 hits from different DOMs we can reconstruct where a particle is coming from. Such a reconstruction is often called an event. In this thesis we are concerned about the runs when ORCA had 4 strings.

1.3 The Moon and Sun cosmic ray shadows

Once finished, these detectors can be used to discover a lot about the universe. While ORCA will mostly be used to find the properties of neutrinos themselves, ARCA is going to look at high-energy objects in the universe. For this neutrinos are useful to observe because the possibility of containing a lot of information about these objects.

The problem is that there is no known neutrino source to cross check the pointing. Because of its depth in the sea there is also no cosmic light reaching the detector. The detector is installed with high accuracy but mistakes can be made at depths of nearly 3000 meters. A cross check is necessary to calibrate the detectors. The lack of calibration could cause artifacts. These are studied in this research, see section 2.2.
The detectors do not only detect neutrinos but are also able to detect muons from cosmic ray interactions and by that detect cosmic rays. These will be blocked by the moon. Just as the moon casts a shadow during a solar eclipse, it also casts a shadow in terms of cosmic particles[6].

Here we determine whether the cosmic ray shadow that is cast by the moon and sun is significantly enough to be detected in the currently available data by ORCA detector. The moon and sun have the biggest angular size in the sky as seen from Earth so they make a good calibration point.

1.4 Goal of this study

In this thesis the matter is often addressed as detecting the moon. But it is important to recognize that the detector only detects particles. The signal addressed in this study is actually a deficit of particles. That would indicate that something blocked the particle in its path to Earth. So although it is technically incorrect, the phrase "detecting the moon" is used for measuring a deficit.

This research is based a lot on research that has been done for other detectors. A few kilometers next to the ORCA detector there is another neutrino detector called ANTARES. It was designed to determine the directional neutrino flux and the search for point-like neutrino sources. In the ANTARES analysis of this topic [6] a similar way of detecting the moon is used as in this research. Another research on this topic was conducted by the IceCube collaboration [7]. The IceCube detector is a large detector that is located in the ice of Antarctica. These larger detectors have been used to detect a deficit of 3σ-10σ significance.

These significant values are not expected in this research because the ORCA-detector is not finished yet. However the goal is to lay a foundation for whenever ORCA is finished. The method described in this thesis for the ORCA-detector is reusable and extendable to other detectors.

This thesis is structured in the following way: In Chapter 2 the theoretical background of this research is explained. After this, in Chapter 3, an analysis on a simulation is done, which is purely based on little empirical results from the ORCA-detector. This part will act as a prediction for the next part, Chapter 4, where we actually look at data from the ORCA detector. In these two chapters first the methods are explained after which the results and discussion come. At the start of the simulation chapter there is also a motivation of why the calibration is important.

Chapter 2

Theory

In this chapter a theoretical basis is laid for the rest of the research. Firstly the used astronomical coordinate systems are discussed together with their implications for this research (section 2.1). After this the theory of mispointing is described (section 2.2). Then the reconstruction of event tracks is explained. This is an integral part of the KM3Net research. However in this research only the basis is explained (section 2.3). Finally the statistical model for counting experiments is described and how it is applied to the obtained data (section 2.4).

2.1 Astronomical coordinates and areas

Looking at the ever-moving universe it is useful to have a well-defined coordinate system. The use of a local Cartesian coordinate system is nugatory; one place on earth has a completely different coordinate system than somewhere else. Not only translated but also rotated. Also the rotation and movement of the Earth needs to be taken into account. In short, a lot of movement to compute. This is why astronomers use astronomical coordinates, or celestial coordinates. These are coordinate systems that are not absolute coordinate systems but have physical reference point.

Every astronomical coordinate system is defined by a primary great circle and a primary point. There are a few combinations that work well [8]. This section explores the two that are used in this research: The horizontal coordinate system and the UTM system.

2.1.1 Horizontal Coordinate System

The horizontal coordinate system (HCS) is the system that is used most in this research. For the HCS the great circle is the observer's horizon. Imagine drawing two linear independent tangent lines to the observer's location on the sphere (or Earth). The span of these two lines make up the horizontal plane. The line that goes directly upward, or more formally, the line that goes radially outward from the centre of the sphere, is called the zenith. The opposite of the zenith, meaning a vector going directly downward, is called the nadir.

The angle an object or event makes with the horizontal plane is called the altitude or elevation. When we speak about an object with an elevation of 90° it is exactly located on the zenith. When the elevation is -90° it is located on the nadir. In this research I mostly use zenith angle, which is the angle from the zenith. In terms of elevation it is $90^\circ - \delta$, where δ is the elevation (see figure 2.1).

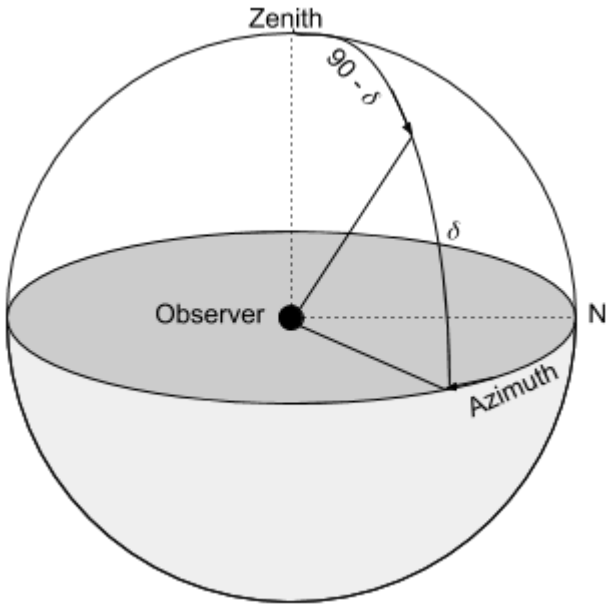

Figure 2.1: *A sketch of the horizontal coordinate system. The elevation is denoted by δ. The north point is shown by N*

The primary point in the HCS is the North Point. This is a point on the horizontal plane that gets constructed by drawing a line from the observer to the North Pole parallel to the horizontal plane. The angle the object or event makes with the North Point line is called the azimuth. It increases clockwise, so the east is at an angle of 90°. All locations on the sphere can

be described with a zenith and azimuth angle. One degree of freedom is dropped due to the fact that we neglect distance from the observer.

The detector measures signals from which a direction of the particles is reconstructed on the unit sphere in Cartesian coordinates. A spherical coordinate transformation is used to transform from a Cartesian system to the HCS. Assuming the x coordinate corresponds with the North Point, and the z coordinate with the Zenith. The resulting transformations are:

$$\delta = \arccos z$$
$$\alpha = 2 \arctan \frac{-y}{\sqrt{x^2+y^2}+x}$$

Here, δ is the zenith angle and α is the azimuth angle. There are two exceptions: When $x < 0$ and $y = 0$ then $\alpha = 180^\circ$. And when both x and y are zero the azimuth is undefined. The $-y$ has as result that the azimuth will be clockwise increasing. If earlier assumptions of the rotation of x, y and z coordinates is correct this transforms them to the right coordinates. However the detector coordinates do not follow this assumption.

2.1.2 UTM System

The coordinate system of the description of position of the moon and the sun is not the same as the coordinate system of the reconstructed events. After transformation to spherical coordinates the reconstructed events are in the Universal Transverse Mercator System, or UTM system. What is important is that the position of events can be described in similar fashion as the in Horizontal Coordinates System. However the primary points are different, and the direction of rotation is counter-clockwise.

The UTM system is primarily used to determine positions on Earth. It has three (or four) parameters: North, East, Zone (and Hemisphere). The Hemisphere variable is optional since it could be included in the North variable. The UTM System projects Earth onto flat map. Although it is topologically impossible to make a flat map from a sphere, the UTM system has a solution. It makes a series of 60 seperate maps, all having a width of 6° longitude[9]. The mentioned Zone parameter defines the map to use.

As can be seen in figure 2.2a, these different maps have parallel longitude lines. But when we would flatten a sphere all longitude lines should converge to one point, for example in the Mollweide Projection (figure 2.2b).

What is important for this research is the transformation from the UTM system to the local HCS. The latter is used to calculate the position of the

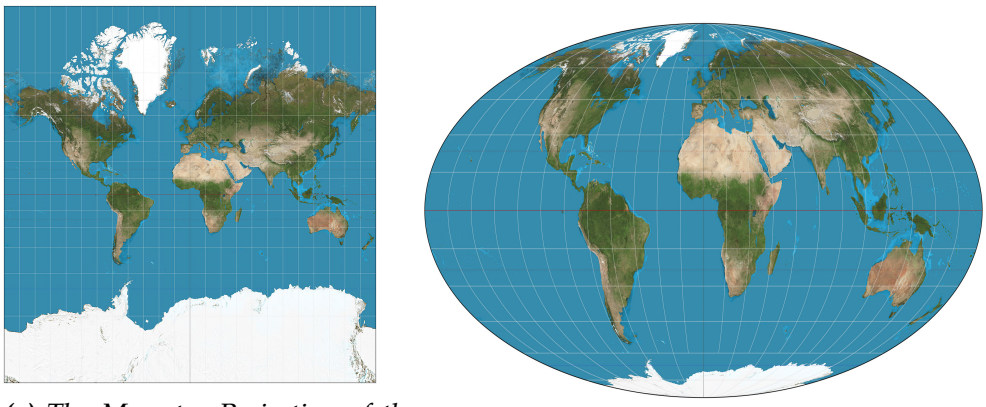

(a) *The Mercator Projection of the Earth [10]*

(b) *The Mollweide Projection of the Earth [11]*

Figure 2.2: *Two projections different projections of the Earth*

moon and sun. The transformation is given as:

$$\delta_{HCS} = \delta_{UTM}$$
$$\alpha_{HCS} = \frac{\pi}{2} - \alpha_{UTM} + \theta_{MCA}$$

Here δ_{HCS} and α_{HCS} are the zenith angle and azimuth angle in the system where the position of the moon and sun are calculated. The first equation is equivalent but the second equation is different. The first term comes from the fact that the x-axis - that was assumed to correspond with the North - corresponds with the East in the UTM system. So a translation of quarter of a circle is appropriate. The second term is the azimuth in the UTM system. The final term, θ_{MCA}, is called the Median Convergence Angle. This angle needs to be implemented due to the fact that in the UTM system the longitudal lines are straight. It is dependent on the Zone and location of the detector. After transformation the positional information of all objects in this analysis are in the same coordinate system.

2.1.3 Area Normalization

For this research the calculation of areas on a sphere is of importance. These areas are used to obtain the number of events per square degree for maps that describe the event density as function of the angular distance to the moon. The division in azimuth in degrees does only at the equator reflect a real degree on the sky, but is much less at higher elevations.

Spherical caps are used to determine the an area, see figure 2.3. The

area of a spherical cap is given as:

$$2\pi r^2(1-\cos\theta)$$

Where θ is the angle from the center of the spherical cap. When subtracting one spherical cap from another we get a ring. This ring is taken to be in steradians and has area:

$$A = 2\pi(1-\cos\theta_2-(1-\cos\theta_1))$$

Where θ_2 is greater then θ_1. From this follows that the area of one of those rings is equal to $2\pi(\cos\theta_1-\cos\theta_2)$ So taking constant steps in $\cos\theta$ we get surfaces of equal area, and hence the event density is properly normalized .

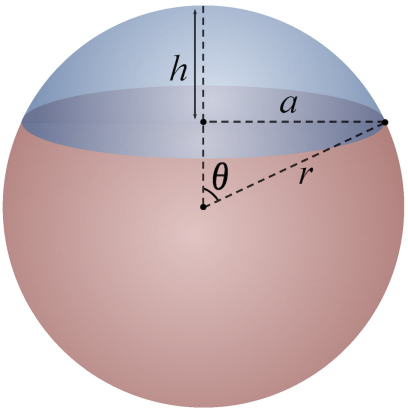

Figure 2.3: *Example of a spherical cap [12]. In this figure θ shows the zenith angle.*

2.2 Mispointing

Perfect pointing is of crucial importance for the study of KM3NeT. That is why the detector should be properly calibrated to have the same coordinate system as it is expected to have. To elaborate, when getting data from the detector certain coordinates are assigned to any reconstructed event. However if the detector is mispointed, the obtained data will not be in the same coordinate system as the algorithms used to analyse the events.

In this research we describe mispointing in the horizontal coordinate system. With the mentioned transformations (section 2.1) the events are converted to the HCS.

The three parameters that describe the mispointing of the detector are:

1. An offset in magnitude from the detector zenith (DZ) from the true zenith (TZ).

2. An offset in direction from the DZ from the TZ with respect to the true north (TN).

3. An offset in direction from the detector north (DN) from the TN.

These parameters are visualized together in figure 2.4a. To elaborate on the three parameters:

1. *The magnitude of offset from the DZ from the TZ*

When this parameter is zero, the zenith-vector of the detector is on the span of the zenith-vector of the true zenith. If this parameter is non-zero the DZ will be slightly tilted from the TZ and this will lead to detection artifacts. In figure 2.4b θ_1 corresponds to the first parameter. It is the angle between the true north and the detector north.

2. *An offset in direction from the DZ with respect to the TN*

When this parameter is zero, the projection of the DZ on the horizontal plane will lay on the span of the TN. When this parameter is increased the DZ will turn clock-wise around the TZ. In figure 2.4c θ_2 corresponds with the second parameter. It is the angle between the projection of the detector zenith on the horizontal plane and the true north. If the first parameter is 0 this parameter has no resulting artifacts. The second parameter describes the rotation of the DZ around the TZ. When the DZ is on the span of the TZ it can not rotate around it.

3. *An offset in direction from the DN from the TN*

When this parameter is zero, the projection of the DN on the horizontal plane, will lay on the span of the TN. In figure 2.4d θ_3 corresponds with the third parameter. The third parameter is the rotation of the horizontal plane of the detector frame. The angle between the TN and the DN tells the rotation around the DZ-axis.

All parameters have their own resulting features in the final result of a measurement. The motivation for this part of the research is to show the influence of mispointing on the result of measuring a celestial object over time.

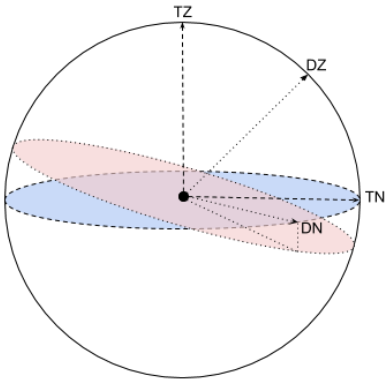

(a) *All three parameters*

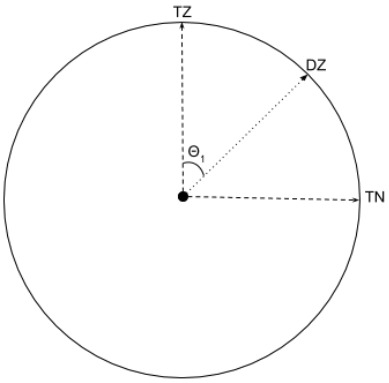

(b) *First parameter θ_1*

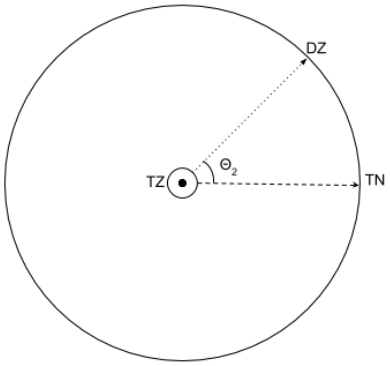

(c) *Second parameter θ_2, TZ points out of the paper*

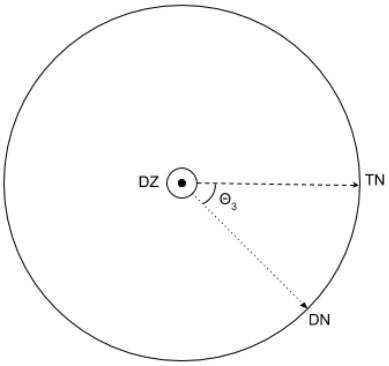

(d) *Third parameter θ_3, DZ points out of the paper*

Figure 2.4: *All three parameters described in 2D figures, TZ is the True Zenith, DZ is the Detector Zenith, TN is the True North and DN is the Detector North*

2.3 Event Reconstruction

Since the PMTs only measure the time of passing the threshold and the ToT, it is difficult for the detector to determine where an event actually comes from. Although the information of multiple PMTs and DOMs tells the difference in arrival time of the Cherenkov radiation, it does not really tell the direction of the moving particle. That is why event reconstruction is a big part of the research for KM3Net. The algorithms used to reconstruct events are beyond the scope of this research. Nonetheless will this section cover the basics because some jargon gets used in later analysis.

2.3.1 The Problem

With the same time offsets between hits, different directions can be deducted. A graphical illustration is given in figure 2.5. This figure will be used for the derivation of the difference in arrival time between two DOMs, shown with the blue circles. The Cherenkov radiation is denoted by the blue arrows.

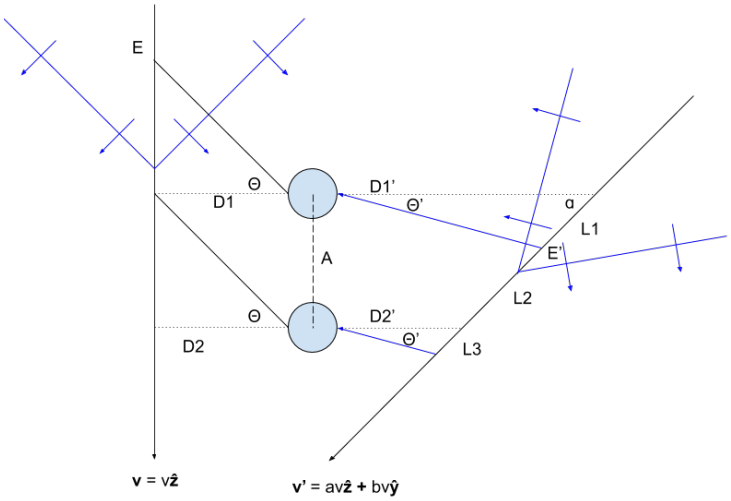

Figure 2.5: *Visualization of same time difference for different directions due to different velocities of the particles*

Time of the vertically moving particle

To only calculate the difference in arrival time of the radiation between the two detectors, $t = 0$ is taken when the particle is in point E. The time for the radiation to hit the first DOM is:

$$t_1 = \frac{R_1}{c} = \frac{D_1}{c \cdot \cos\theta}$$

Where R_1 is the distance traveled by the light from the the point of radiation. The time for the radiation to arrive at the second DOM is:

$$t_2 = \frac{R_2}{c} + \frac{A}{v} = \frac{D_2}{c \cdot \cos\theta} + \frac{A}{v}$$

But $D_1 = D_2$ so the difference in arrival time will be:

$$\Delta t = t_2 - t_1 = \frac{A}{v}$$

Time of the diagonally moving particle

For the diagonal line some parameters need to be specified first. These parameters cancel or become 1 in the latter derivation but not in the general case:

Parameter α is the angle that the track of the particle makes with $D1'$ and $D2'$. In the vertical case this was equal to 90°. This is determined with the velocity of the particle, which is a scaled and rotated version of the vertical line:

$$\tan\alpha = \frac{av}{bv} = \frac{a}{b}$$

Note that a, b could be more than one combination. The difference in time is calculated in a similar way as before. First R_1' is determined, which is again the distance traveled by the light from the point of radiation. This is done with the law of sines:

$$\frac{R_1'}{\sin\alpha} = \frac{D_1'}{\sin\pi - \theta' - \alpha} \rightarrow R_1' = \frac{D_1' \cdot \sin\alpha}{\sin\pi - \theta' - \alpha}$$

$$t_1' = \frac{D_1' \cdot \sin\alpha}{c \cdot \sin\pi - \theta' - \alpha}$$

Note that the vertically moving particle also follows this formula when $\alpha = \frac{\pi}{2}$. For the second time we first need to find a relation between D_1' and D_2'. Since the lines are parallel, the following equation is true:

$$D_2' = D_1' - \frac{A}{\tan\alpha}$$

Version of June 22, 2020– Created June 22, 2020 - 15:07

A similar expression is found for the radiation part of t'_2:

$$t'_2 = \frac{(D'_1 - \frac{A}{\tan\alpha}) \cdot \sin\alpha}{c \cdot \sin\pi - \theta' - \alpha}$$

This way the time difference is not dependent on either D'_1 or D'_2 because for the difference in the time the radiation takes is now:

$$\Delta t' = t'_2 - t'_1 = -\frac{A \cdot \cos\alpha}{c \cdot \sin\pi - \theta' - \alpha}$$

Note that this is the difference in travel time of the radiation not the actual time difference. Again this collapses to the vertical case when $\alpha = \frac{\pi}{2}$, then it becomes 0. Now the only addition has to do with velocity, which the detector does not know a-priori. Hence the difference in arrival time for both scenario's could be the same because

$$\frac{A}{v} = \frac{A'}{|v'|} - \frac{A \cdot \cos\alpha}{c \cdot \sin\pi - \theta' - \alpha}$$

depends on v'. This velocity depends on a and b. The ratio between a and b determines α, but the magnitude of these variables are free to choose. So there are multiple values that satisfy this equation. This motivates the point that it is difficult to determine where events are coming from.

2.3.2 The solution

Luckily there is a solution. This is done by a clever algorithm that are fabricated by KM3Net[13]. The algorithm initially hypothesises N directions where the event could come from. This leaves some parameters to be fitted, these are the position and the time at which the event crosses some reference plane that is perpendicular to the direction. These parameters are fitted in an iterative way. Every iteration tries to minimise the χ^2 which is based on the time difference between the actual time and the expected time for the photons arrival. The directions with the lowest value for χ^2 have the highest probability of being the 'correct' parameter. These are send to next stage.

In this stage the algorithms takes the likeliest directions and scans around them to find even better solutions. In the end the algorithm should find a global minimum and takes this as most likely direction the particle could come from.

How good or likely the fits are, is given by the likelihood parameter Q. This variable is used a lot in this research because it makes it possible

to make quality cuts. High likelihoods indicate the level of consistency of the track hypothesis with the detected signals. Since the likelihood scales with the amount of hits on PMTs, the hits are also saved and are used to divide the likelihood later on.

2.4 Counting statistics

To make a useful conclusion for this research, counting statistics is needed to tell if a deficit of events is really significant. Although this theory is straightforward, it is a fundamental part of this research.

m experiments have results: $N_1, N_2 \dots N_m$. In counting statistics, if the measurements are big, $N_i >> 10$, the measurements will approximately follow a Gaussian distribution:

$$P(N) = \frac{1}{\sqrt{2\pi}\sigma} \exp - \frac{(N-\mu)^2}{2\sigma^2}$$

The average can be estimated by the sample average:

$$\mu \approx \overline{N} = \frac{1}{m} \sum_{i=1}^{m} N_i$$

All individual measurements are from a binomial distribution, an event or not an event. For small p the expressions for the average and the variance are given:

$$\overline{N} = pN$$
$$var(N) = pN(1-p) \approx pN = \overline{N}$$

So the distribution for the counting experiment is:

$$P(N) = \frac{1}{\sqrt{2\pi\overline{N}}} \exp - \frac{(N-\overline{N})^2}{2\overline{N}}$$

In this study only smaller amounts of events from the moon and sun are expected. To determine a certain p-value to this measurement N the definition of the p-value is needed: $P(n \leq N) = \alpha_0$, which roughly translates to: what is the probability of finding the same or lower value for a certain measurement N.

To make the statistics a bit simpler we will introduce a variable transformation: $N \rightarrow \frac{N-\overline{N}}{\sqrt{\overline{N}}}$. This transformed variable is normally distributed with $\mu = 0$ and $\sigma = 1$. The transformation also tells the significance in terms of σ.

Version of June 22, 2020– Created June 22, 2020 - 15:07

The p-value is calculated with the Cummulative Distribution Function (CDF). This function is often non-analytic and values are found numerically. In this paper the CDF of the Gaussian distribution is used which is often denoted with capital letter Φ. The CDF assumes that the input value is distributed normally with $\mu = 0$ and $\sigma = 1$, hence:

$$p = \Phi(\frac{N - \overline{N}}{\sqrt{\overline{\overline{N}}}})$$

In this research an average is calculated from so called 'off-target' measurements*. With this average the probability of a certain deviation can be determined.

*This terminology is explained later on. For this section it is not important

Version of June 22, 2020– Created June 22, 2020 - 15:07

Chapter 3

Simulation

This chapter starts with the motivation for this research by looking at the artifacts that arise from mispointing. After this a section is dedicated to simulation of the position of the moon and the sun. With the created information a plot is created. This is done with a realistic assumption of the angular resolution and measured event densities on these positions. This will serve the purpose of quantifying the expectation for the signal in the current ORCA data. This chapter also contains discussion of the method and results. Future research on some topics is also suggested.

3.1 Mispointing

The positions of the moon in a given time were calculated using a program by Clancy James based on SlaLib[14] routines [15]. It was used as a tool to visualize what happens when mispointing a detector. The program calculates the expected location of the moon with as input the 3 parameters from section 2.2. This expected location is compared to the real location of the moon.The pseudo-code can be found in the Appendix (6.1).

As output it gives three 2-dimensional maps all focused on the moon*. The three maps show the moon in three different ways. The first is showing the position of the centre of the moon relative to the expected centre of the moon. The second one shows the amount of events blocked by the moon and the last shows how the detector would reconstruct these blocked events. The latter is useful for researching the effect of the angular resolution.

*The sun can also be implemented in this code, but originally it was written for the moon

The intention of this analysis is to perform a qualitative evaluation of the artifacts arising from mispointing.

3.1.1 Method and results

The effect of the three parameters described in section 2.2 are separately evaluated. For every parameter several simulations are done for a day (01-01-2008) using constant time steps. Different values for this parameter are evaluated.

Null measurement

Figure 3.1 shows the resulting map of the event deficit. A circle on the spot the moon is visible. Rays from random positions are send 'towards the detector' so not every coordinate will count the same amount events.

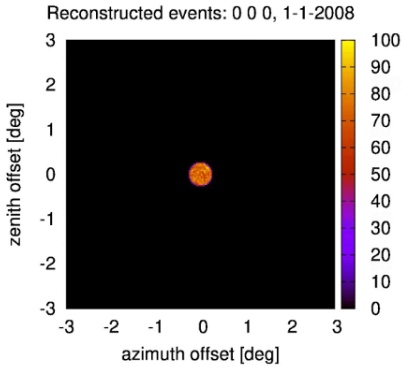

Figure 3.1: *This figure shows the number of events blocked as function of the distance in azimuth and zenith direction (values in z-axis) for perfect pointing.*

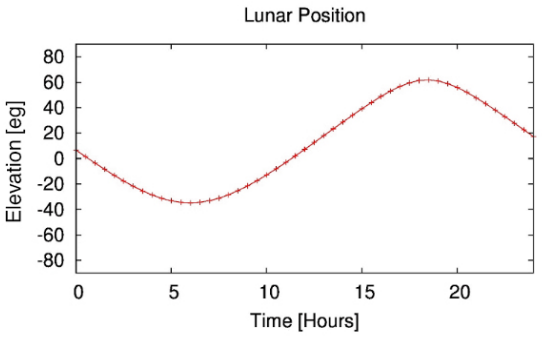

Figure 3.2: *Elevation of the moon over the course of 1 January 2008*

Figure 3.2 shows the elevation of the moon during the day. This has no influence when there is no case of mispointing. When there is a mispointing in the detector the elevation of the moon is of importance.

First parameter: Magnitude of offset from the zenith

Figure 3.3 visualizes the effect of the first parameter. In the figure the center of the moon is shown. Showing the centre makes it clear how the moon moves due to mispointing. The z-axis indicate the time the moon is at that particular point relative to the expected location of the moon. The curve is not closed because for an observer on the Earth the moon does not rotate a perfect 360° within a solar day.

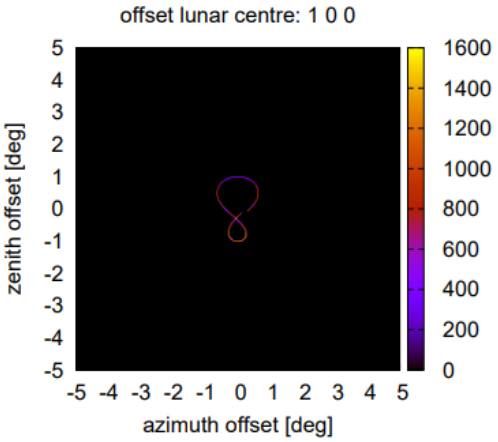

Figure 3.3: *The time (denoted in the z-axis) the center of the moon spends on a certain location relative to the expected moon's center when the first parameter of mispointing is 1°*

In the figure it is visible that the first parameter acts on the apparent movement of the moon. The reason that the top part is wider than the bottom part is because of the elevation of the moon. A mispointing in azimuth of a constant value has a different impact at different elevations as explained in section 2.1.3. When the curve is in the origin in figure 3.3 the elevation of the moon is 0 in figure 3.2. When the parameter is given different values, see figure 3.5 and figure 3.4, it does not change its shape. It just gets magnified or mirrored. The behaviour stays the same.

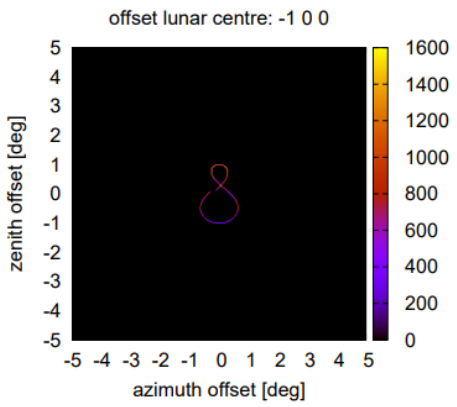

Figure 3.4: *The time (denoted in the z-axis) the center of the moon spends on a relative location of the expected moon when the first parameter of mispointing is -1°*

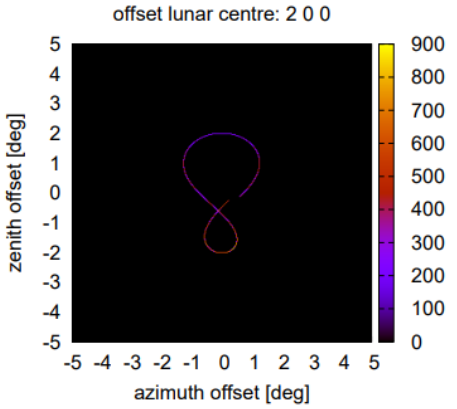

Figure 3.5: *The time (denoted in the z-axis) the center of the moon spends on a relative location of the expected moon when the first parameter of mispointing is 2°*

Second parameter: Direction of offset

As stated in section 2.2, the second parameter needs the first parameter to have an impact. In these results the first parameter is 1 for this reason.

Figure 3.6 shows the results for the direction of offset being 180°. The z-axis shows the time the moon is at that location. It is the same result as in Figure 3.4. This is expected because a rotation of 180 degrees is the same as mirroring in the True Zenith.

Different artifacts arise when the second parameter is changed to 45° (3.7), 90° (3.8) and 135° (3.9). Now the curve that traces the centre of the moon takes a different shape. 90° (figure 3.8) is the symmetry value. An offset parameter of $90° + \alpha$ is the mirrored version of $90° - \alpha$. It is a curve consisting of two parabolas. The 'size' of the parabolas is determined by the suprema of the elevation. The bigger parabola corresponding to the highest elevation in figure 3.2 and the smaller one with to lowest elevation.

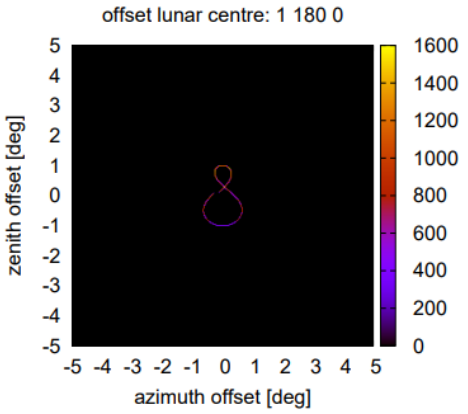

Figure 3.6: *The time (denoted in the z-axis) the center of the moon spends on a relative location of the expected moon when the second parameter of mispointing is 180°*

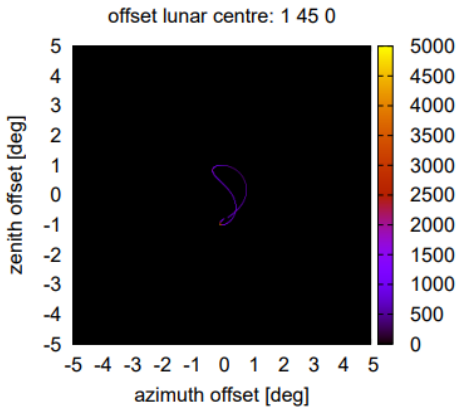

Figure 3.7: *The time (denoted in the z-axis) the center of the moon spends on a relative location of the expected moon when the second parameter of mispointing is 45°*

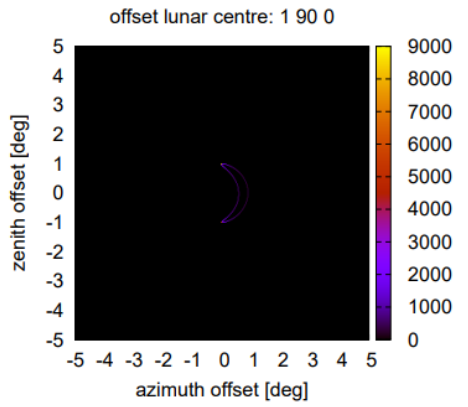

Figure 3.8: *The time (denoted in the z-axis) the center of the moon spends on a relative location of the expected moon when the second parameter of mispointing is 90°*

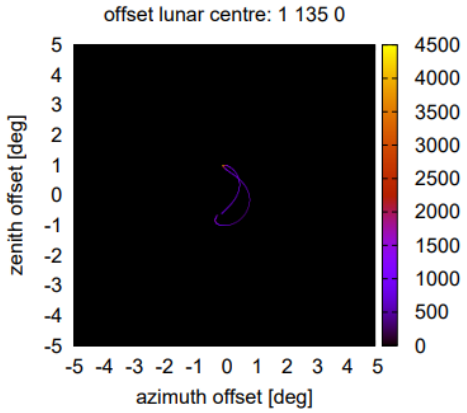

Figure 3.9: *The time (denoted in the z-axis) the center of the moon spends on a relative location of the expected moon when the second parameter of mispointing is 135°*

Third parameter: Offset of the detector north

The final parameter is visualized in figures 3.10a, 3.10b and 3.10c. In these figures the number of blocked events is shown on the z-axis. In the figures the location of the moon changes during the day. The distance from the origin is dependent on the elevation (figure 3.2). Although it is not much, it is visible that this effects reduces when the moon has a bigger elevation. The moon is closer to the origin in figure 3.10c and 3.10b where the absolute value of the elevation is bigger than for figure 3.10a.

3.1.2 Conclusion

This part of the research was meant for qualifying the behaviour of the results when mispointing the detector. I can conclude that the results motivate the importance of calibrating the detector to have the exact same coordinate system as it is expected to have. Because it is not only a matter of locating an event at a different spot, the result also smears out. There is no fixed location of where events came from over time. When multiple particles come from the same source at a different time, the detector would not measure them consistently in the right spot. The analysis also demonstrates that for the identification of mispointing it is necessary to evaluate the moon signal separately for different elevations.

In the results section the artifacts that arise when the first and third parameter are combined are lacking. This would have been a good indication if the parameters are independent of each other.

These observations can be used in future studies. The ARCA detector will look at high-energy objects in the universe. A perfect calibration is necessary for this research. A study that could be done is that the three parameters are fitted to a certain observation by iterative changing on a expectation value of the three parameters. This way the offset of any detector can be found.

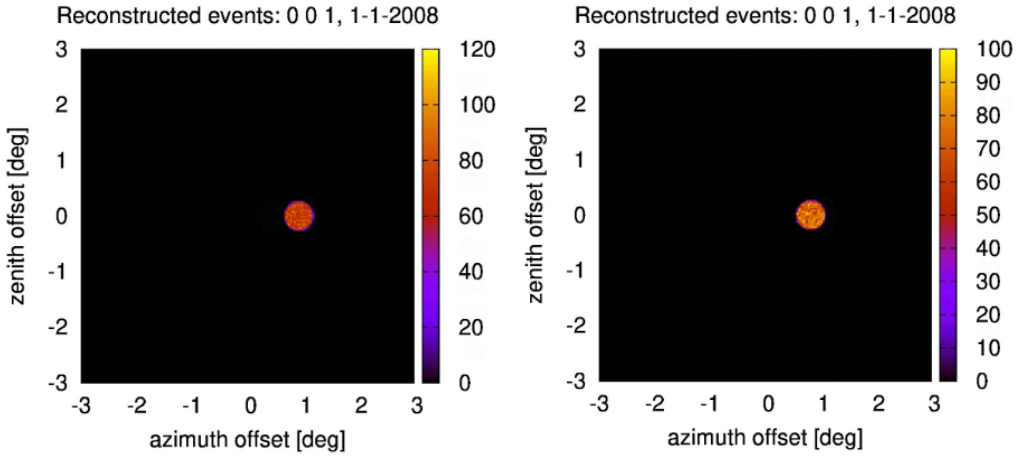

(a) *This is taken on 01-01-2008 at 0:00* **(b)** *This is taken on 01-01-2008 at 5:00*

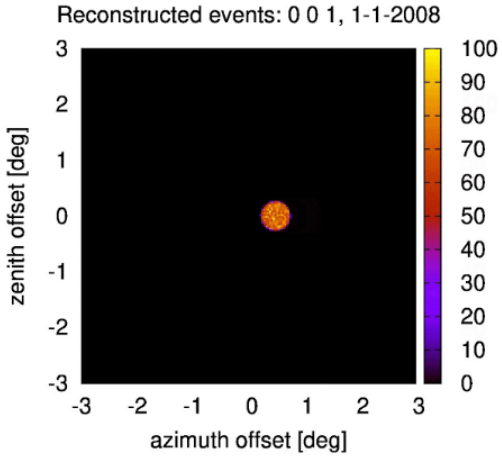

(c) *This is taken on 01-01-2008 at 18:00*

Figure 3.10: *These figure shows the number of events blocked at the relative position of the expected location of the moon (values in z-axis) when the third parameter of mispointing is 1° taken at different times. The elevations of the moon at the mentioned times are shown in figure 3.2*

3.2 Simulation of ORCA

Now that mispointing is qualitatively analysed it is time to look at what to expect for the study of real data. It is useful to make a prediction for the data that is analysed later. In this part the detector is perfectly pointed so there are no mispointing artifacts.

The begin of this section will be about the event density that is measured with the ORCA detector. With this event density plots of the neighbourhood of the moon for an entire year are created. This shows a total amount of expected events from and around the moon. Assuming that all events are blocked that came from behind the moon, a statistical prediction is made of what would happen for the real data. This assumption gives realistically the highest significance. In the study of the actual data a lower significance is expected. Besides this an analysis of the impact of the angular resolution of the detector has on the final statistics is made.

3.2.1 Event density

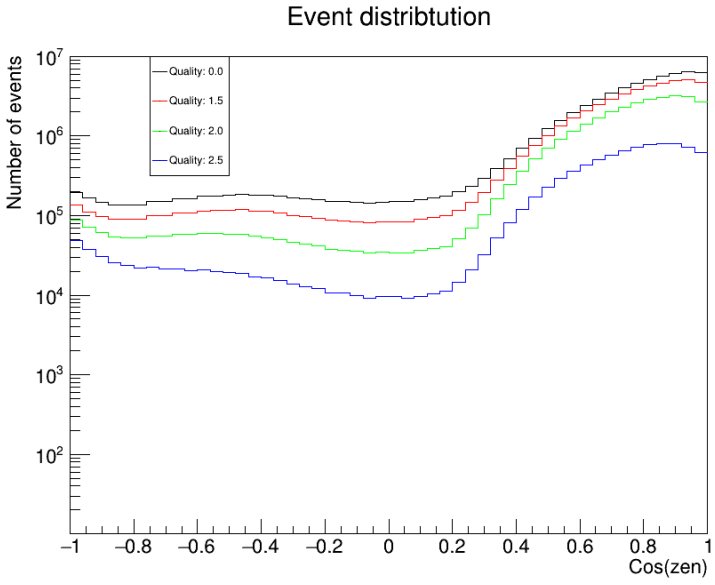

Figure 3.11: *The number of events as function of* cos *zen measured by the ORCA-detector. The events are from runs between 23 July 2019 and 25 January 2020.*

First a background is created with the number of events in the neighbourhood of the moon for a year. The script from section 3.1 calculates the position moon is at a certain time. Only the implementation of the event

density at that zenith is needed. This event density is close to constant for every azimuth[†] but it is not for different zeniths.

Figure 3.11 shows how much the event density changes with zenith. For bins of equal area the events are shown as function of $\cos zen$, whereby $\cos zen = 1$ corresponds to the events straight from above. The different lines correspond with different quality cuts (section 2.3). For this analysis the quality cut is 2 so the green line in the figure is used.

First a linear regression model for the measured event density is created. The motivation for this is that the script only takes analytical values to speed up the process. The following model is used:

$$\log y = \sum_{n=0}^{6} a_n \cdot x^n$$

Where y is the number of events on a certain zenith $cos(zen)$. a_n is the linear fit parameter and x is equal to $\cos zen$. The logarithm is there because the y-axis in 3.11 is in a logarithmic scale. The following formula determines the fit parameters[16]:

$$\hat{\beta} = (X^T X)^{-1} X^T Y$$

$$\hat{\beta} = \begin{bmatrix} a_0 \\ a_1 \\ \vdots \\ a_6 \end{bmatrix} Y = \begin{bmatrix} Y(x_0) \\ Y(x_1) \\ \vdots \\ Y(x_{bins}) \end{bmatrix} X = \begin{bmatrix} 1 & x_0 & x_0^2 & \dots & x_0^6 \\ 1 & x_1 & x_1^2 & \dots & x_1^6 \\ \vdots & \vdots & \vdots & \ddots & \vdots \\ 1 & x_{bins} & x_{bins}^2 & \dots & x_{bins}^6 \end{bmatrix} \tag{3.1}$$

Using the data from figure 3.11, the values in 3.1 are found. Plotting the polynomial with these parameters and the initial data gives figure 3.12. Fitting well enough for this analysis purposes. Note that the x-axis is flipped in figure 3.12. So in this case $\cos zen = -1$ corresponds to events coming from above.

n	a_n
0	3.057
1	2.269
2	-6.889
3	-3.654
4	3.692
5	-1.188
6	3.799

Table 3.1: *Fit parameters of linear regression of the number of events as function of zenith from figure 3.11*

With this analytical event density the mentioned program can determine the amount of events for every zenith in the script. All

[†]This is not the case for the ORCA detector yet as with only 4 strings the efficiency has an azimuthal dependence, but for simulation purposes we assume that the event density is constant in azimuth.

events whose origin is below the horizon are
ignored. In the analysis on the real data this will also be the case.

The script calculates the zenith of the moon for every minute of a year. At this calculated zenith a 2-dimensional plot of 10° by 10° is created. For every zenith in the plot the amount of events for a minute are calculated with figure 3.11. After this the program sums everything over the course of a year.

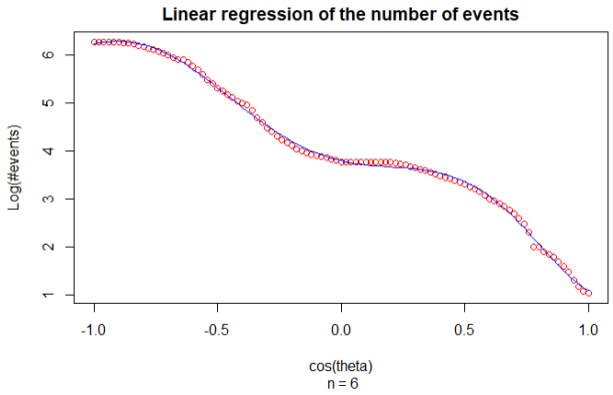

Figure 3.12: *Linear regression model for the event distribution of figure 3.11 by using the parameters in table 3.1*

3.2.2 Results

Figure 3.13 shows the map of events in the neighbourhood of the moon for an entire year. A gradient result arises from the different zeniths in the map. The smaller zeniths have a bigger event density. A lower zenith angle means it will be more towards the zenith, so it is higher in the sky.

The average amount of events in a year is around 1440 per square degree (1.6ev/bin in the binning of 3.13). Suppose the moon blocks all the events that originate from behind the moon. And the moon has an angular radius of about 0.25°

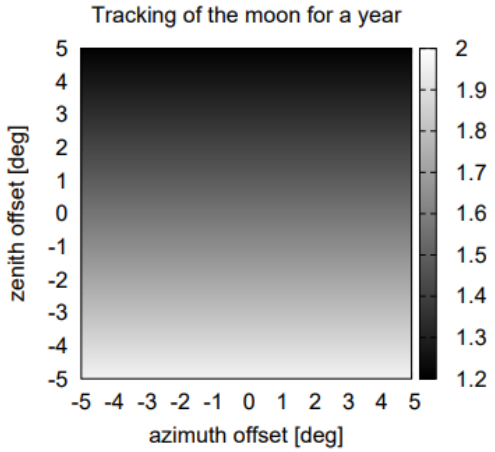

Figure 3.13: *Number of events in the neighbourhood of the moon simulation of a year. 300 bins in the azimuth direction and 300 bins in the zenith direction*

meaning its angular area is about 0.19 square degree. Then the moon will block about 294 events.

With the counting statistics of section 2.4 a significance of $\frac{294}{\sqrt{144000}} = 0.77\sigma$ is found. The p-value of this measurement is:

$$p_{moon} = \Phi(\frac{-275}{\sqrt{144000}}) = 0.22$$

This is result is not significant enough to state that something is blocking events. Only when the significance is 5σ it can be stated that this would be the case. With more time the lack of events gets more significant. The significance also depends on the patch size. The influence of this is analysed later in this chapter.

It is not taken into account that the moon changes in angular size with this method. Although the significance will not improve a lot if this would have been implemented, it would be a proper addition to this simulation. This can be done in follow-up research on this simulation. This will make the simulation more true to what happens in reality. For this research it was left out because only a rough prediction of the significance was enough.

Furthermore is it expected that for the real analysis the significance is lower because we assumed a consistent background. Besides the assumption that the moon blocks all events is made while in reality this not necessarily true. With all assumptions this is the highest significance obtainable while still being partly true to reality. In future research the impact of these assumptions can be determined.

3.2.3 The Sun

When also looking at the sun, twice the statistics could be obtained in the same time. The sun has a similar angular size as the moon as seen from Earth. Using the same method, we can also derive the amount of events blocked by the sun. Calculating the location of the sun for an entire year we evaluate a similar map with the events around the sun.

The plot for the sun can be found in figure 3.14. Now the average is 1575 events per square degree. The total amount of events comes out to be 157500. Assuming that also the sun blocks all events we obtain an amount of $157500 - 332$. The corresponding significance for this lack of events is 0.83σ and the p value is equal to 0.20. This is a very similar result as for the moon. This is expected since the they have the same angular size and similar elevations.

When combining the results of the two the significance increases it is assumed that the moon and the sun plots do not share events. This would happen in reality when the moon an when there is a solar eclipse.

Now the significance is 1.14σ and the p-value is:

$$p = \Phi(\frac{-626}{\sqrt{301500}}) = 0.13$$

With this method the errors of the fit parameters of the linear regression of the background data are not taken into account. Doing this would give a upper- and lower-bound to the significance. The reason for leaving it out, is that this part of the research is meant for giving a rough prediction.

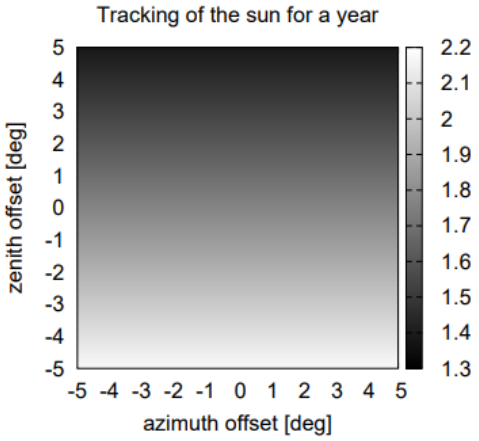

Figure 3.14: *Number of events in the neighbourhood of the sun by a simulation of a year. 300 bins in the azimuth direction and 300 bins in the zenith direction*

3.2.4 Angular Resolution

For every device of measuring light or particles the angular resolution is of importance. First of all it is important that a clear image is created of what we want to measure. But higher resolution also improves the significance of the measurement as well.

In the previous section it is mentioned that the significance depends on the size of the map. This can be done if it is assumed that deficit of events by blocking forms a cylindrical hole. As a result of angular resolution this is not the case. Here we want to show the expected shape of the deficit in the maps.

Starting with the program of Clancy James[15] where we measured the event density. As assumed in the previous section, the moon and sun will both block all events that originate behind it. But now we do not assume that the lack of events due to the moon and sun form a well. They are normally distributed.

Method and results

The program takes the same event density as in figure 3.11. The position of amount of missing events are distributed with a Gaussian distribution.

For the variance some empirical results are necessary. Figure 3.15 showing the expected angular resolution as determined in simulation. There are a few things to note, the first is that the $cos(\theta)$ corresponds to the direction of movement of the event. For this analysis the x-axis is multiplied by -1 to find the origin of the event. Secondly, the median is to be the standard deviation for my Gaussian distributions. This means that the actual resolution is better than in this simulation because 39% of all events are within 1 sigma of a 2D Gaussian.

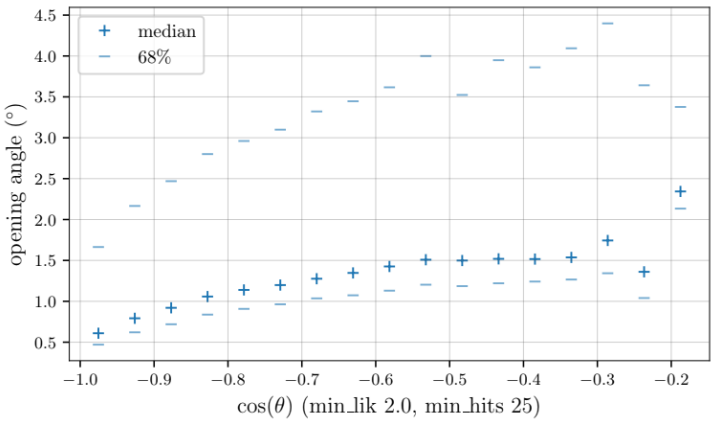

Figure 3.15: *The angular resolution of the ORCA detector as function of* cos *zen [17]*

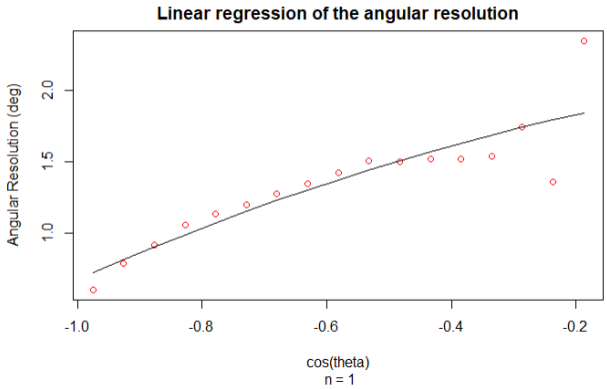

Figure 3.16: *Linear regression of the median from figure 3.15*

To implement this angular resolution in the analysis a linear regression of figure 3.15 is made. This is shown in figure 3.16. After this, an angular resolution map that, for every time step, created a Gaussian surface with a standard deviation corresponding to the proper zenith angle was computed. All the surfaces are added and scaled so that the volume below this surface is the same as the amount of expected missing events.

This method results in the event density that can be seen in figure 3.17. This plot is similar to figure 3.11. When creating a 3D plot of the event density and look from the side (figure 3.18) a small dent in the surface is visible. This dent will get deeper and narrower when the angular resolution gets smaller.

If the angular resolution were lower the moon analysis could focus on a smaller patch and the same amount of missing events would lead to a more significant detection. For example using a patch with side length would result in an average amount events of 23040. But we would still miss 294 events. This gives a significance of 1.9σ. When making the plot even smaller, this significance would even increase more. However there is a limit, because the plot should not be smaller than the moon or sun itself.

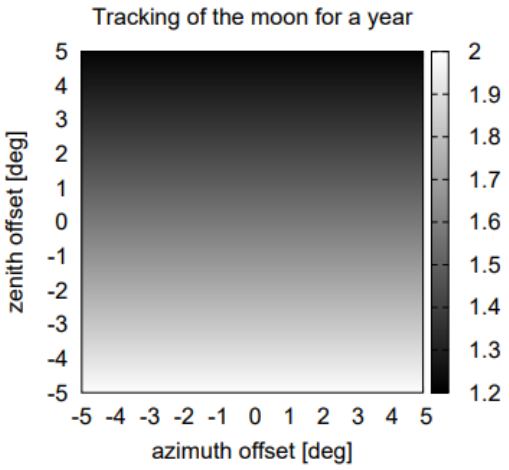

Figure 3.17: *Number of events in the neighbourhood of the moon simulated for a year. 300 bins in the azimuth direction and 300 bins in the zenith direction*

This chapter is mainly intended to give predictions and to show the importance of mispointing. A lot can be improved on these simulations. This is already mentioned in the chapter. A followup research would be to look at the moon and sun on certain zeniths. The moon and sun cover some elevations more than others, looking at specific elevations will give insight on how this coverage affects the measurements. Furthermore, this entire simulation is deterministic. If we would like to imitate actual results there should be some randomness in the plots. This could be implemented by taking the events at random from a distribution that is determined from the emperical event density, figure 3.11.

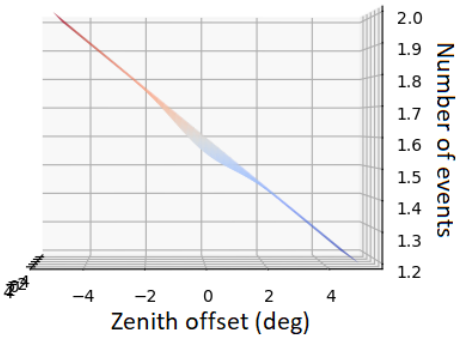

Figure 3.18: *Figure 3.17 viewed from the side to show the deficit of events in the middle*

Chapter 4

Real Data

This chapter focuses on the analysis of the data that is provided by the ORCA4 detector. ORCA4 means the ORCA detector when it only had 4 strings installed. The time over which the data was taken is from 23 July 2019 to 25 January 2020. And the total amount of events measured during that time is 83.5 million.

First the general distributions in local azimuth and zenith coordinates of the detector are evaluated. These distributions contain the information of the origin of the events and positions of the moon and sun. With time offsets for of the moon and sun so-called 'fake moons' are created. These 'fake' sources follow the same path in the sky as the moon and the sun in terms of azimuth and zenith. But they are time shifted. They thus do not contain any signal but should contain similar systematics as the real source. With an analysis of these offsets a general average amount of events is computed. Comparing the on-target measurement to this average gives the significance of the deviation of the amount of events.

4.1 General Distributions

The first part of this chapter is focused on the event distribution and the location of the moon and sun in the entire coordinate space of the detector. This gives a expectation for the event distribution in the neighbourhood of the moon and sun. The expectation is that the amount of events coming from above is bigger than the amount of events coming from below. When particles traverse the earth they have a chance to get blocked. This chance is small for neutrinos compared to other particles because neutrinos do not interact a lot. But these measurements of the detector contain all events

and where they come from. This suggests that most particles come from above.

In figure 4.1 the event distribution for all zenith and azimuth angles is shown. These coordinates are in the HCS of the ORCA detector. This is the same system as the locations of the moon and sun are calculated in. The z-axis shows the number of events in each bin. As expected, lower zenith angles have more events than higher angles. This means that the coordinate system described in 2.1 is well defined.

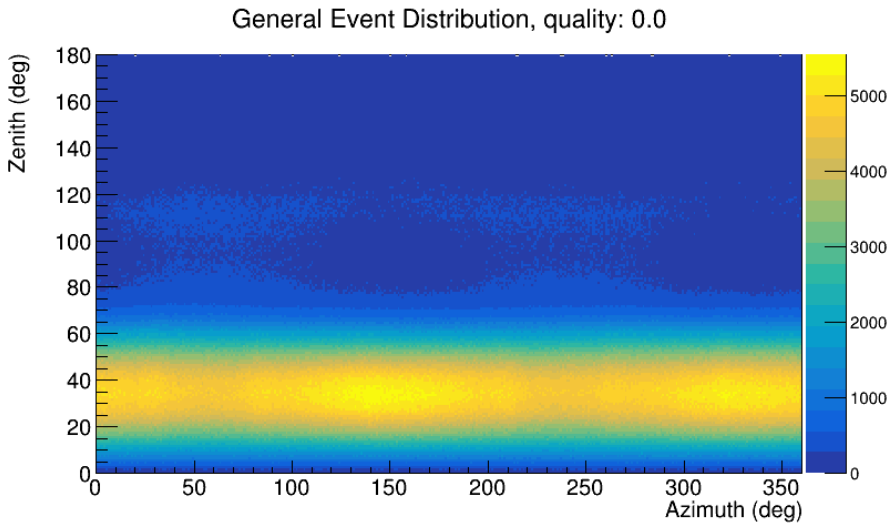

Figure 4.1: *The event distribution for the zenith and azimuth angles for the specified time, quality cut : 0.0. The binning is 360 by 180*

The amount of events near the zenith is decreasing in this coordinate system. This is not due to the fact there are less events*, but this is due the binning in equal azimuth distances, which results in having a smaller real area covered in the bins of high elevations(section 2.1.3) .

Furthermore the event density is not constant in the azimuth direction. This means that the detector is an-isotropic. So for evaluating background sky patches that are equivalent to the patch around the moon it is not possible to take an offset of a certain amount of degrees in the azimuth direction. For the azimuth the event density changes. So in this research time offsets are used rather than a position offsets to determine an average number events in a sky patch.

Quality cuts have an influence on the number events that are analyzed. In figures 6.1, 6.2 and 6.3 (These can be found in Appendix 6.2.1) the other

*We expect most events coming from straight above

quality cuts are shown. The range of the z-axis show that the total number of events decreases. But the shape of the distribution stays the same as for the 0.0 quality cut (figure 4.1). The distribution of the events is similar as in the the one for 4.1. This suggests that the algorithm described in section 2.3 treats the events the same for different zenith angles.

Furthermore the zenith and azimuth angles the moon and the sun cover during the the measuring time is analyzed. Due to the location of the ORCA detector it is expected the moon does not rise above and set below certain elevations. The same reasoning applies to sun as well. From figure 4.2a and 4.2b we can see the expected zenith and azimuth angles of the moon and sun. The cause of the holes in the moon plot are unknown but are suspected to be due to binning. The reason for the different range on the z-axis, which represents the time in 10 seconds, is caused by the moon having more positions that it covers for a long time.

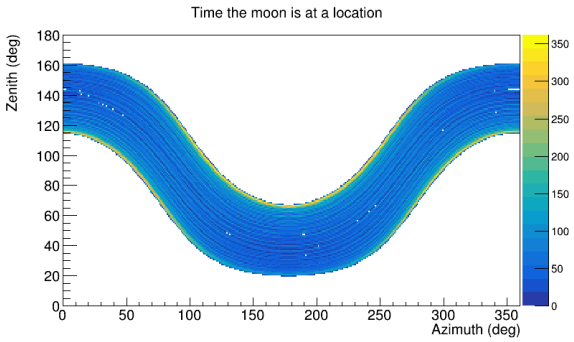

(a) *The moon*

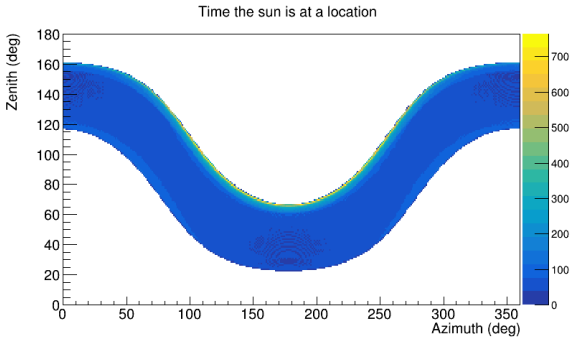

(b) *The sun*

Figure 4.2: *The amount of time for which the moon and the sun are visible within the specified time period shown as function of azimuth and zenith at the ORCA site*

With these qualitative results we progress to the actual event densities around the sun and the moon. And start measuring whether there are significantly less events around these celestial objects.

Version of June 22, 2020– Created June 22, 2020 - 15:07

4.2 1-Dimensional Analysis

This section is dedicated to one dimensional analysis. In this analysis only the number of events as function of the angular distance to the moon and sun matter. This section will be split in a method section and two sections for the results of the moon and the sun. In the latter the results are discussed and suggestions for further improvement are provided.

4.2.1 Methods

There are several things that are established before the actual analysis is done. First of all a way to determine where the moon and the sun are at every moment in time is necessary. This is done by using a lookup-table. This table contains the location of the moon and sun relative to the ORCA-detector at every tenth second. Since the events start at 23 July 2019, this is chosen to be the epoch. Meaning that at time 00:00 we start measuring the position of the sun and moon until a day after the last event has occurred in timesteps of 10 seconds. I took a margin of a day because later on in the analysis we would like to determine 'off-target' measurements. This is done by taking a time offset of two hours. Moreover on this later.

With SlaLib[14] routines the location of the moon and the sun in the sky in terms of azimuth and zenith is determined. This table (4.1) is then stored in a document that is accessed by the analysis program.

TimeIndex	Moon_Azimuth	Moon_Zenith	Sun_Azimuth	Sun_Zenith
0	(0,360)	(0,180)	(0,360)	(0,180)
1	⋮	⋮	⋮	⋮
2	⋮	⋮	⋮	⋮
⋮	⋮	⋮	⋮	⋮
1632959	⋮	⋮	⋮	⋮

Table 4.1: *Layout of the lookup table for the moon and the sun*

The ranges of the variables are indicated by the values in the parentheses. Note that the TimeIndex column means: $TimeIndex \cdot 10s$ since the epoch (23-07-2019 00:00:00). This means that the entire table covers a time of 16329600 seconds, which is 189 days. The way this table can be accessed is by taking the time of the event relative to the epoch. This relative time is used to determine the coordinates from the moon and sun.

Next is determining where the events come from. This is done with the coordinate transformation from section 2.1. After these transformations they are in the same coordinate system as the lookup-table entries.

As well as the origin of the event the likelihood is also stored. Which is determined by the total quality of the event divided by the number of PMTs that are hit by the event (see 2.3). Hence the table has the form of table 4.2. With these two tables (4.1 and 4.2) all useful information for this

Time	Azimuth	Zenith	Quality	Hits
(Unix Timestamp)	(0,360)	(0,180)	(0,→)	(0,→)
⋮	⋮	⋮	⋮	⋮
⋮	⋮	⋮	⋮	⋮

Table 4.2: *Layout of the table the contains all the events, one row for every event*

research is stored.

The first analysis is of the 'off-target' measurements determining whether they form a significantly constant background. We can then compare the 'on-target' measurement with this constant background. These 'off-target' measurements are created by offsetting the event time by a certain amount of time. In this research the time offset increments with two hours because the moon is moving with about 360°in 24 hours, which corresponds with 15°in an hour. This means that two neighbouring hours share events, which will make them correlated.

Event density around the sources

For every offset we will iterate over all events and determine the angular distance of each event to the moon and the sun. The angular distance is determined with the formula:

$$D = \arccos \mathbf{r_{event}} \cdot \mathbf{r_{Moon}}$$

Here $\mathbf{r_x}$ corresponds to unit vector of the event and the moon or sun. If the likelihood is bigger than the quality cut the event is counted as an entry with distance D. For this research 4 quality cuts are used: 0.0, 1.5, 2.0 and 2.5. The total amount of histograms obtained is: $12(offsets) \cdot 4(qualities) \cdot 2(moon/sun) = 96$ histograms. Typical and selected ones with striking features will be shown in this thesis. All off-target plots can be found in the Appendix.

Before we get on to the results, one more thing needs considering. Since the time interval between the events are not constant and I will use the

times the fake sources are above the horizon, $zen < 90$, not every offset gets the same 'chance' to get the same amount of events. This requires scaling of the off-target measurements.

The scaling will work in the following way. First we iterate over all offsets and check for every event the zenith angle of the source. It is stored in a histogram that has a domain of $[0, 90]$. Thus obtaining 12 histograms that contain the number of times the source was on certain zenith during the times of the events. These histograms are multiplied with the normalized event distribution as function of zenith angle.

In figure 4.3 this normalized event distribution is shown (quality 0.0). The others can be found in the Appendix (figures 6.4, 6.5 and 6.6). Then, for every offset, multiply the number of times the moon spends at a certain zenith angle with the normalized amount of events at that zenith. The sum of all these products gives a so-called 'chance' variable. The ratio between the chance variable and the average is a scaling factor for the number of entries in an offset. This gives all offsets the same 'chance' to get the same amount of entries for its plot, hence we can analyse the statistics more accurate. Of course, this scaling process also applies to evaluation of the sun. In the next section I will show the results of this process.

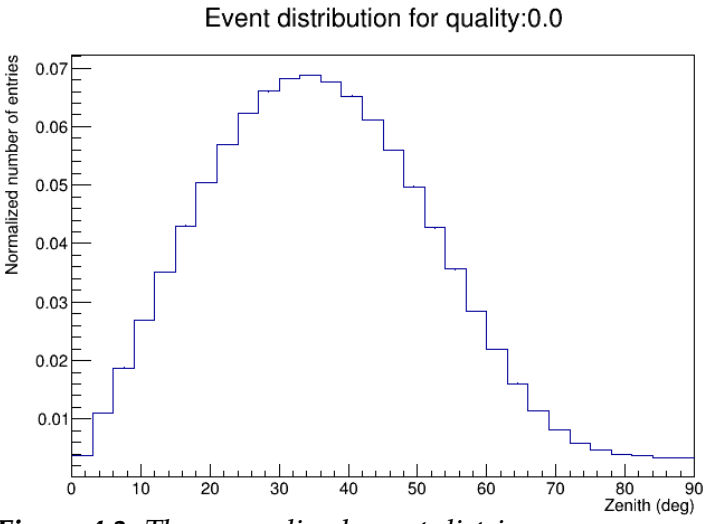

Figure 4.3: *The normalized event distribution for each zenith smaller than 90°, quality: 0.0*

4.2.2 Results

This results section will be split in to two parts. The first part will concern the moon and the second part will concern the sun. Combining the results could result in a more significant result, see section 3.2.4. For both I will start with analyzing the scaling of the amount of events. After this I look at the number of events as function of the distance to the source. First will be the analysis of the offset measurements. This determines if there is a constant background. Using this background knowledge we look at the actual moon and sun and determine if it is statistically visible.

The Moon

First the scaling of the amount of events in the histograms is demonstrated. In figure 4.4 the amount of entries before checking if all the offsets had the same 'chance' variable is shown. Together with the calculated number of entries for each offset. A deviation between the offsets is visible.

The calculated number of entries and the actual data have the same behaviour. The ratio between the blue line and the average of the blue line used will be determined to scale the real amount of entries. In figure 4.5 the number of entries for the scaled offsets are shown. In figure 4.5 a oscillating pattern is visible. In a further study it could be determined where this oscillation comes from. It oscillates twice when increasing to an offset of a day.

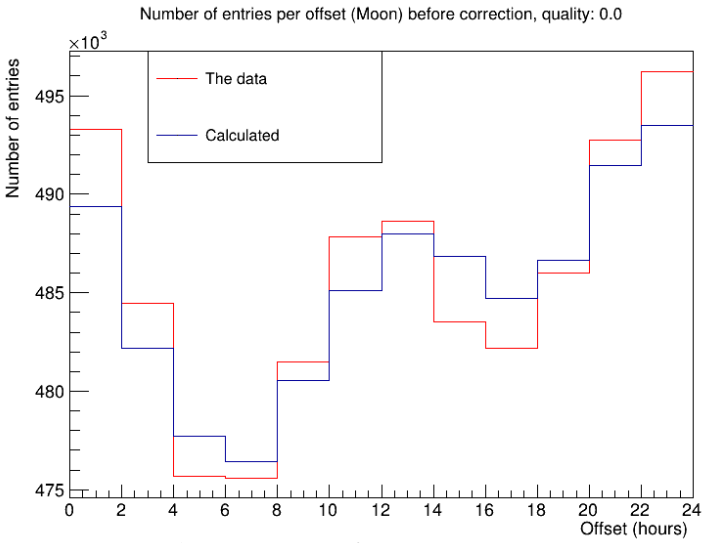

Figure 4.4: *The amount of entries per offset when it does not normalize it*

The average of the number of entries for this particular quality cut (0.0) is equal to 485629 events. Applying the counting statistics from section 2.4 gives a standard deviation of $\sqrt{485629} \approx 697$. The 2σ interval is between the values 487023 and 484235. Statistically 95% off the measurements for this data should be inside this interval if the measurements are taken from the same distribution.

The offsets are deviating with the highest value in figure 4.5 is 489088

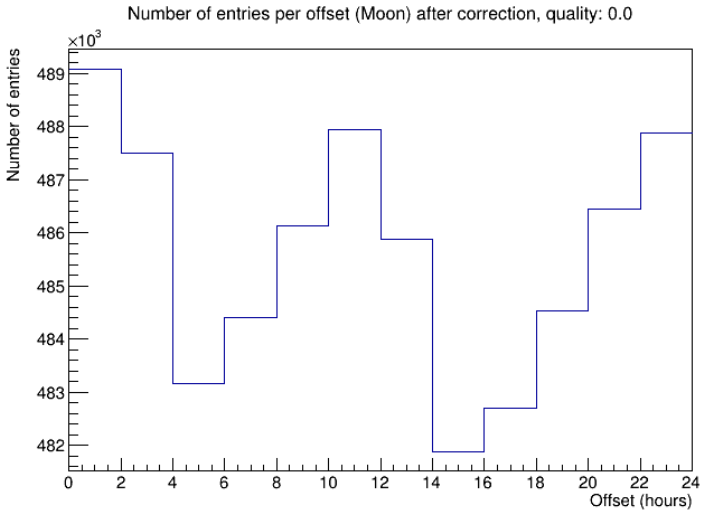

Figure 4.5: *The amount of entries for every neighbourhood of the fake moons when the correction factor is taken into account. Quality: 0.0*

and the lowest value is 481880. These values correspond with a significance of 4.96σ and 5.38σ respectively. These outliers may indicate some remaining systematic flaw in the correction.

The number of events per square degree as function of the distance to the moon are evaluated. For this we divide the area around the moon into different rings. This area is calculated with spherical caps (section 2.1.3). Using the small angle approximation for the cosine and a constant bin width the following formula for the area is found.

$$A(\theta,\delta) = 2\pi(\cos(\theta-\delta)-\cos(\theta))$$

$$\approx 2\pi(1-\frac{(\theta-\delta)^2}{2}-1-\frac{\theta^2}{2})$$

$$= \pi(2\theta\delta-\delta^2) = \pi(2\cdot i\cdot\delta^2-\delta^2)$$

$$A(i,\delta) = \delta^2\pi(2i-1)$$

Where i is the number of the bin, δ is the width of a ring.

A typical distribution after area normalization can be seen in figure 4.6. The red line corresponds with the average and the two dotted red lines indicate the 1σ interval. The first value has the largest standard deviation and fluctuates a lot for different offsets. This is a consequence from this bin having the smallest area and with this the lowest amount of events.

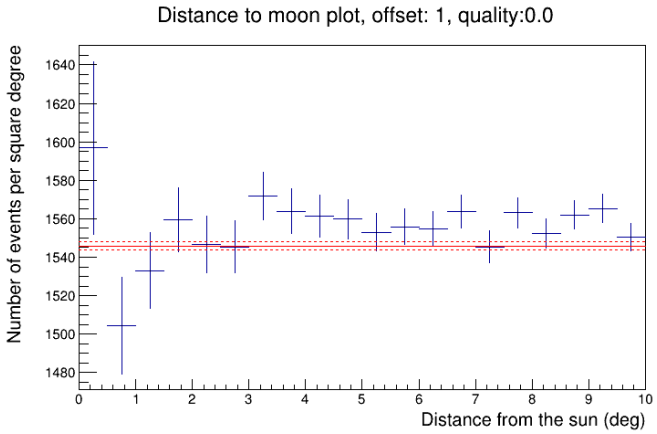

Figure 4.6: *Number of events per square degree as function of the distance of the moon for all events and no quality cuts are applied, offset: 1*

The consistency of the data with a model of flat background is now quantified via an evaluation of the corresponding χ^2:

$$\chi^2 = \sum_{i}^{bins} \frac{(x_i - average)^2}{(std_i)^2}$$

Here x_i corresponds to the value of bin i and std_i corresponds to the standard deviation of this bin. If we do this sum for the plot above we find $\chi^2 = 40.8$. The number of degrees of freedom corresponds to the number of bins. The probability of having this or a higher χ^2 value corresponds then to 0.004. We now repeat this method of finding the χ^2 values for all the offsets and qualities.

For every quality cut a plot is made with the probability that the data is consistent with the average background for the four qualities (0.0, 1.5, 2.0, 2.5). These can be seen in figure 4.7, 6.7, 6.8 and 6.9 respectively as the blue points. The latter three can be found in the Appendix. These χ^2 probabilities with respect to a constant background average are to low to state that there is a consistent background in the time offsets of the moon background.

Fit parameter	1555.4
χ^2	16.7
$p(X > \chi^2_{19})$	0.61

Table 4.3: *The fit parameter, χ^2 statistic and the probability of that statistic for the data of figure 4.6 compared to a fitted flat line.*

Now we will determine whether the data for a source is consistent with any flat line fit on the data of this source. This flat line is used to compute the χ^2 statistic. For figure 4.6 the relevant information of this analysis is shown in table 4.3.

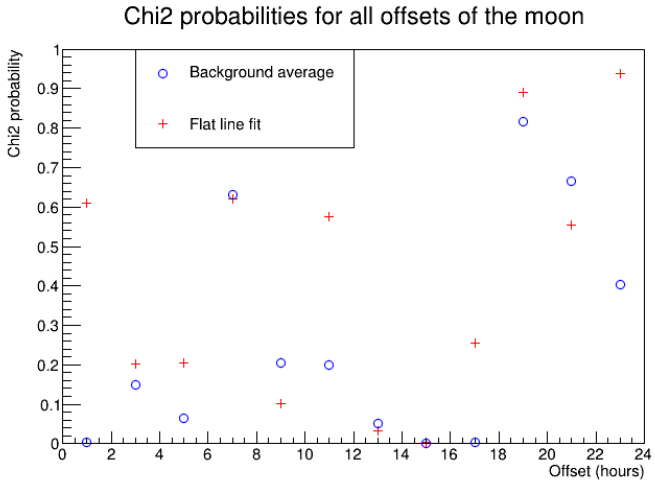

Figure 4.7: *The χ^2 probabilities of the data for all the offsets of the moon compared to the average background and to the fitted background, quality 0.0*

Repeating this method for all offsets and no quality cuts applied gives the red crosses in figure 4.7. This same method but with quality cuts applied gives the red crosses in figures 6.7, 6.8 and 6.9 in the Appendix.

The probabilities of the data with respect to a fitted line are generally higher comparing with the same offset source data compared to a constant background average. But the data of some off target sources is still not consistent with a flat line. If the hypothesis of the background being consistently flat is true then with more statistics all the probabilities should increase because the number of events per square degree should converge to an average. However in this analysis this has not been found.

As mentioned, the average background computed by the off-target measurements is not a good estimate for the background of the moon. This means we can not compute an average to determine whether the number of missing events around the moon is significant.

Quality	Fit parameter	χ^2	$p(X > \chi^2_{19})$
0.0	1553.8	28.5	0.07
1.5	1281.3	24.9	0.17
2.0	861.8	24.7	0.17
2.5	250.5	18.6	0.48

Table 4.4: *The fit parameter, chi^2 statistic and the probability of this statistic for the data of all the quality cuts of the on-target measurements of the moon*

However it is still instructive to look at the on-target measurement of

the moon. In figure 4.8 the number of events per square degree as function of the distance to the moon is shown. Quality cuts on this data are shown in figures 6.10, 6.11 and 6.12.

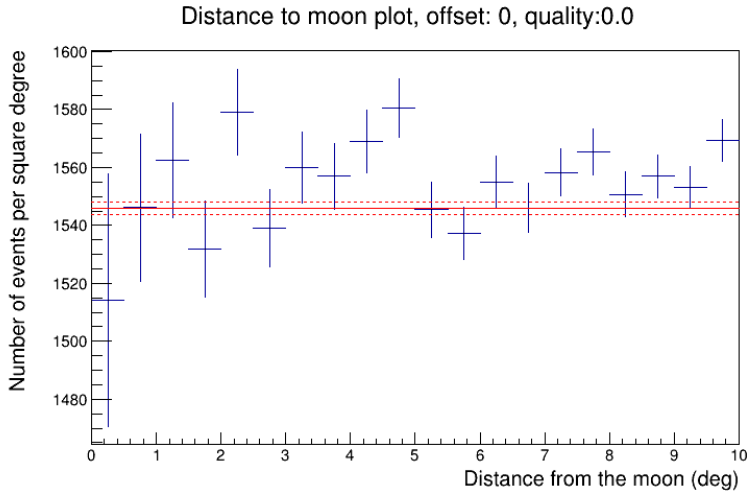

Figure 4.8: *The number of events per square degree as function of the distance to the moon. No quality cuts are applied. The red line indicates the average background of off-source measurements. The dotted lines is* 1σ *interval.*

The information about the flat line fit to the different quality cuts can be found in table 4.4.

We can compare the results of the on-target measurements to the predictions made in section 3.2.4. In the Simulation section the average number of events per square degree for a quality cut of 2.0 was equal to 1440 events per year. With the actual data we find this value to be equal to be 861.8 events in 189 days. Scaled to a year this ends up to be 1664 events per squared degree. This difference might be caused by several factors. Some of these factors are discussed in section 3.2.4.

The Sun

For the sun I perform the same analysis as for the moon. Starting with the amount of events around the off target sources of the sun.

The normalized entries can be seen in figure 4.9. This is in contrast with what is expected based on the results in the simulation section (3.2.4), where the number of events around the sun was bigger than for the moon.

The average amount of events per offset is equal to 348532. This implies that the standard deviation is 590. The the upper and lower bound of the 2σ interval are 349713 and 347351 respectively. The highest and lowest

Version of June 22, 2020– Created June 22, 2020 - 15:07

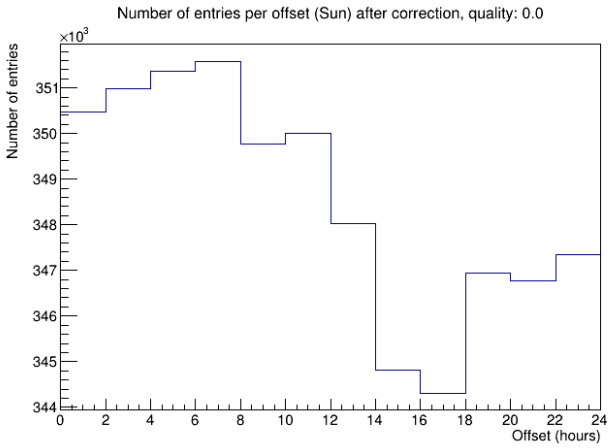

Figure 4.9: *The amount of entries for every neighbourhood of the fake suns when the correction factor is taken into account. Quality: 0.0*

total number of entries of are 351586 and 344391. These values correspond with a significance of 5.17σ and 7.01σ.

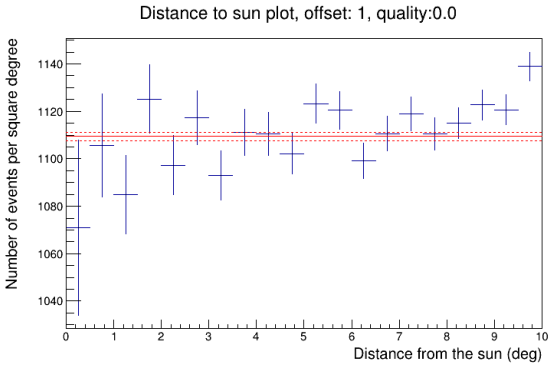

Figure 4.10: *Number of events per square degree as function of the distance of the moon for all events and no quality cuts are applied, offset: 1*

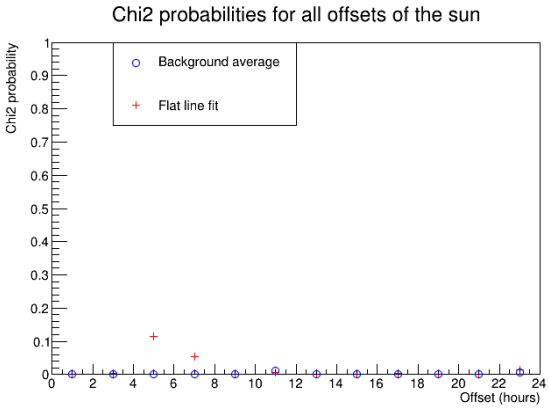

Figure 4.11: *The χ^2 probabilities of the data for all the offsets of the sun compared to the average background, quality: 0.0*

In figure 4.10 the plot of the data for the off-target source that is offsetted by 1 hour is shown. The information about the consistency of the data with respect to a background average is shown in table 4.5.

The probabilities of the data for all off-target sources with respect to a background average is shown in figures 4.11, 6.13, 6.14 and 6.15 (the latter three can be found in the Appendix) with the blue points. These figures show that the data for the background of the sun is not consistent.

The data for each off-target measurement is fitted to a flat line. The information of the consistency of the data of 4.10 compared to a fitted line is also shown in 4.5. For all off-target sources the probabilities are computed. For no quality cuts these probabilities are shown as red crosses in figure 4.11. The probabilities for all off target sources compared to a flat line fit for the different quality cuts are shown in figures 6.13, 6.14 and 6.15 with the red crosses.

Average background	1109
χ^2	49.5
$p(X > \chi^2_{20})$	0.0002
Fit parameter	1115.8
χ^2	47.8
$p(X > \chi^2_{19})$	0.0002

Table 4.5: *The fit parameter, χ^2 statistic and the probability of that statistic for the data of figure 4.10 compared to an average background and a fitted flat line.*

Although it is not possible to analyze the deficit of events in the on-target measurement of the sun compared to a constant background because of the systematic errors, it is still instructive to show the figures and statistics. In figure 4.12 the number of events per square degree as function of the distance to the sun is shown when no quality cuts are applied. The figures for the other quality cuts can be found in the

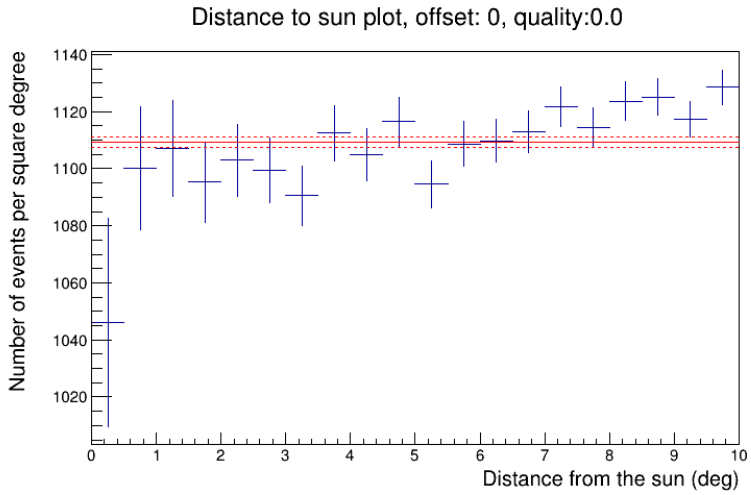

Figure 4.12: *The number of events per square degree as function of the distance to the sun. No quality cuts are applied. The red line indicates the average background of off-source measurements. The dotted lines is 1σ interval.*

Appendix (figure 6.16, 6.17 and 6.18). The consistency of the data with a constant average background are found in 4.6. Also the consistency of the data with a flat line fit are found in this table.

This analysis shows that the data of the sun is not consistent with a flat line. With the comparison to a constant average background and a flat line fit the χ^2 statistic is high and the probabilities are low.

Quality	0.0	1.5	2.0	2.5
χ^2 with constant average	39.1	45.0	45.6	27.7
$p(X > \chi^2_{20})$	0.006	0.001	0.001	0.12
χ^2 with flat line fit	48.4	53.3	55.7	28.6
$p(X > \chi^2_{19})$	0.0002	4.2e-5	1.6e-5	0.07

Table 4.6: *chi^2 statistic and the probability of this statistic for the data of all the quality cuts of the on-target measurements of the moon compared to a constant average background and a flat line fit.*

As mentioned in section 3.2.4 the combined statistics result in a better significance. But first a consistent value for the average should be established. In follow-up research the systematic error in the correction could be discovered. This should allow to measure a consistent background. When this is established the significance of the deficit of particles in the neighbourhood of the moon and sun can be determined.
Another research could be to consider more offsets. This analysis could give information about the systematic error in the correction factor. If the is determined the correct way then the statistics should be increased. This is done by waiting for the detector to measure more events. The influence of time can be studied by taking a subset of the current data.

4.3 Linear event density

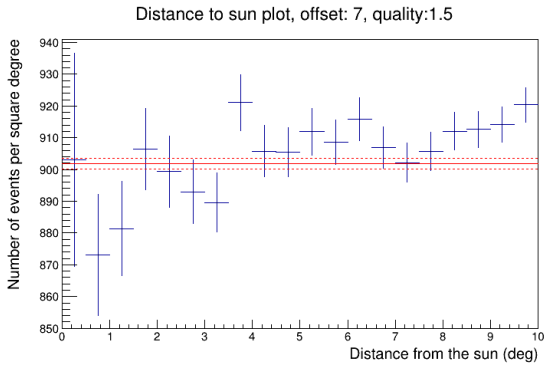

Figure 4.13: *Event density as function of the distance of the sun, offset: 7 & quality: 1.5*

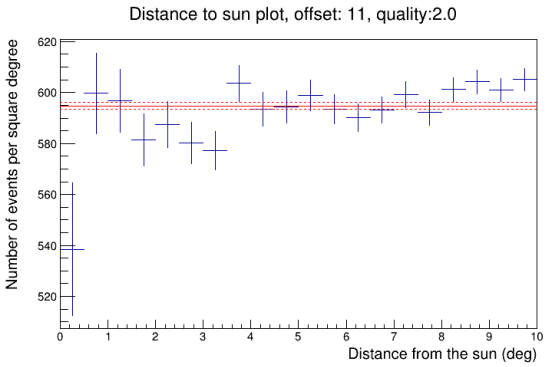

Figure 4.14: *Event density as function of the distance of the sun, offset: 11 & quality: 2.0*

In figures 4.10, 4.13 and 4.14 a slope is visible. The latter two are chosen to show that this is not due to quality cuts or offsets but all off-target measurements are in the Appendix. In the previous section we found that the data for the off-target measurements is not consistent with a fitted flat line. However it might follow a linear background.

The approach will be fairly similar to the constant background that was used in the previous sections. Now a linear regression is done over all the data points of the off target sources for either the moon or the sun. This will create a linear model of the average number of events as function of the distance to the sun. After this we can again calculate the χ^2 probabilities for every off-target measurement.

4.3.1 The Sun

First a linear regression is done over all data of the off-target sources. The result is plotted in figure 4.15. The parameters of the linear regression

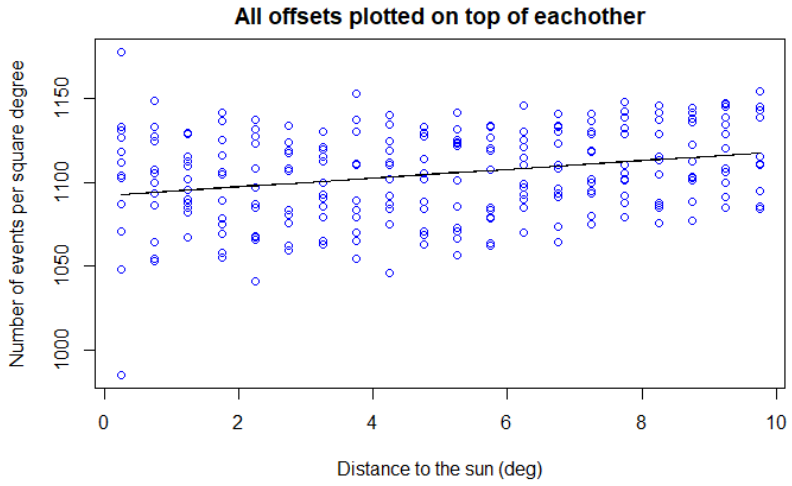

Figure 4.15: *Linear regression over the data of all off-target measurements of the sun, quality: 0.0*

are $a = 2.77$ and $b = 1092.56$, corresponding to the slope and intercept respectively. The χ^2 statistic is now calculated with:

$$\chi^2 = \sum_{i}^{bins} \frac{(x_i - (ax + b))^2}{(std_i)^2}$$

Where x_i and std_i correspond to the value and the standard deviation of a bin. x_i is the location of the center of bin i. The χ^2 statistics for the three figures mentioned at the start of this section are shown in table 4.7. The

Figure	χ^2 average background	χ^2 linear background
4.10	49.5	29.4
4.13	43.2	27.0
4.14	33.1	19.7

Table 4.7: *χ^2 statistic when the data of figure 4.10, 4.13 and 4.14 are compared against an average background and a linear background.*

probabilities increase accordingly as can be seen in figure 4.16. Here the probability of the linear background is shown with the red crosses. As comparison, the background average is shown with the blue points. The

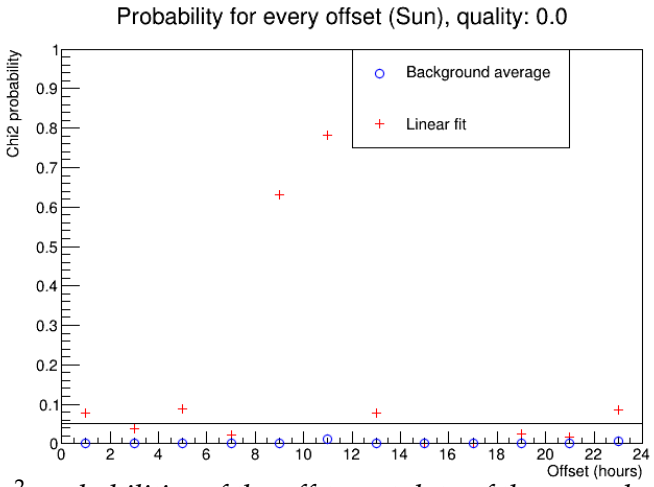

Figure 4.16: *χ^2 probabilities of the off-target data of the sun when compared to an average background and a linear average with slope 2.77 and intercept 1092.56, quality: 0.0*

same kind of analysis is done for all the other qualities. In table 4.8 all the calculated fit parameters can be seen.

Quality	a	b
0.0	2.77 ± 0.6	1092.56 ± 3.7
1.5	2.20 ± 0.5	888.47 ± 2.9
2.0	1.38 ± 0.3	586.33 ± 1.9
2.5	0.65 ± 0.2	165.23 ± 0.9

Table 4.8: *Fit parameters of the linear regression of all the data of off-target sources of the sun*

All the corresponding χ^2 plots can be found in the Appendix (figure 6.19, 6.20 and 6.21). It is visible that for all the analyzed quality cuts the consistency of the data with respect to a linear average increases.

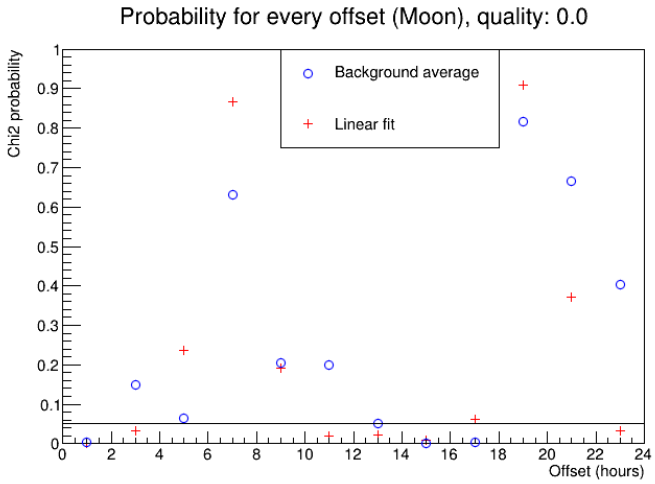

Figure 4.17: *χ^2 probabilities of the off-target data of the moon when compared to an average background and a linear average with slope 0.87 and intercept 1538, quality: 0.0*

4.3.2 The moon

It is instructive to make the same analysis for the moon. Table 4.9 shows the fit parameters of the linear regression. The slope parameters is smaller than it is for the sun, especially for the latter two qualities. Applying the same method for calculating the χ^2 statistics and comparing them to a χ^2_{18} distribution the probabilities are computed. In figure 4.17 the χ^2 probabilities are plotted with the red crosses. The other qualities can be found in the Appendix (6.22, 6.23 and 6.24 The linear fit did not increase the probabilities in the linear regression model 4.17 comparing to 4.7. The difference between the constant and linear background is not that significant.

Quality	a	b
0.0	0.81 ± 0.6	1537.35 ± 3.4
1.5	0.32 ± 0.5	1269.45 ± 2.8
2.0	-0.07 ± 0.4	856.81 ± 2.1
2.5	-0.06 ± 0.2	250.12 ± 1.0

Table 4.9: *Fit parameters of the linear regression of all the data of off-target sources of the moon*

4.3.3 Difference moon and sun

The linear behaviour arises from the zenith angle coverage for the moon and the sun. In figure 4.18 zenith coverage by the sun and moon during the time of the runs is plotted. The sun has a sharper and higher peak around 65°, while the moon spent more time at lower zenith angles than the sun.

Version of June 22, 2020– Created June 22, 2020 - 15:07

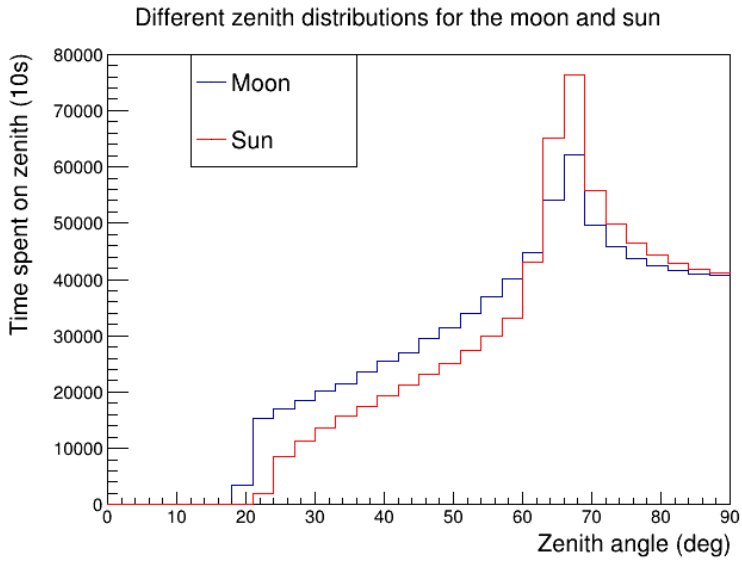

Figure 4.18: *The time the moon and sun spend at a certain angle*

This directly affects the number of events as function of distance to these objects. Figure 4.3 shows the normalized event distribution as function of the zenith angle. These two figures together (4.18 and 4.3) explain why the sun has a bigger slope in the number of events per squared degree.

When the sun is at an 65°zenith angle, the detector measures events in the range from 55°to 75°. If the event distribution would be linear locally there, it would give flat event density. Meaning $E(55°) - E(65°) = E(65°) - E(75°)$, where $E(zen)$ is the event distribution as function of zenith (figure 4.3).

In figure 4.3 it is visible that the event density is non-linear in certain zeniths. This can result in either a increasing or decreasing slope in the event density as function of the distance. The three possible scenario's for a certain zenith angle are:

$$\begin{aligned} E(\alpha - 10°) - E(\alpha) &= E(\alpha) - E(\alpha + 10°) \\ E(\alpha - 10°) - E(\alpha) &> E(\alpha) - E(\alpha + 10°) \\ E(\alpha - 10°) - E(\alpha) &< E(\alpha) - E(\alpha + 10°) \end{aligned}$$

These (in)equality's correspond with a constant, sloping upward and sloping downward event density for that zenith angle (α) respectively.

To determine whether the final event density as a function of the distance to the moon or sun has a slope, the slope for every bin of figure 4.3

is determined with equation: †

$$(E(\alpha - 10^\circ) - E(\alpha)) - (E(\alpha) - E(\alpha + 10^\circ)) \tag{4.1}$$

These values are multiplied per zenith with the corresponding value from figure 4.18. Using this method figure 4.19 is found. Summing for all

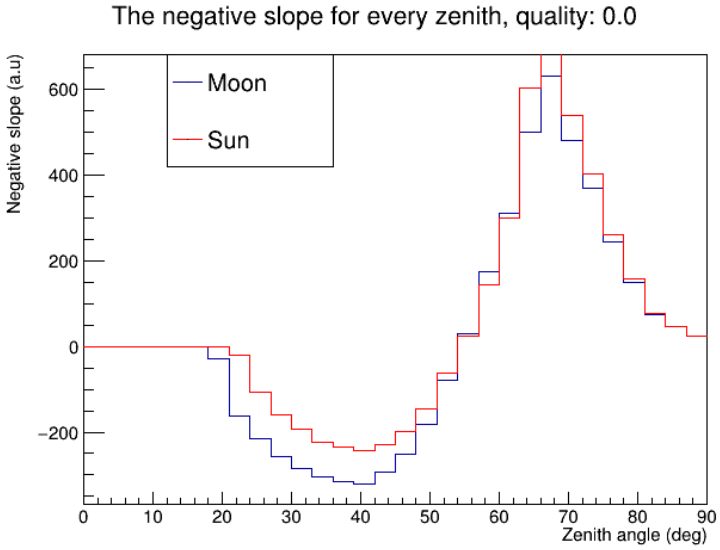

Figure 4.19: *The negative slope for for every zenith determined by equation 4.1, multiplied bin by bin with figure 4.18. Quality: 0.0*

zeniths we obtain the values 344 and 1541 for the moon and sun respectively. The value for the sun is a lot higher resulting in bigger slope for the number of events per square degree as function of the distance to the sun/moon. For other qualities the results are noted in table 4.10.

Quality	Moon	Sun
0.0	344	1540
1.5	324	1609
2.0	265	1656
2.5	103	1545

Table 4.10: *The sum of the bins of 4.19, for every quality*

Although the values do not directly translate in the slope of the corresponding event density, the method shows that there is some correlation. Since the slope of the moons event density is consistently lower than the suns.
Figure 4.19 shows that the sum first will decrease, becoming negative. After this it will increase and become positive at some point. It is obvious that there is some zenith angle where the sum will be zero. If this happens the

†Note that when $\alpha < 10^\circ$ this will cause problems. This is solved by then assuming $\alpha - 10 = 0$. The same applies for when $\alpha > 80^\circ$

Version of June 22, 2020– Created June 22, 2020 - 15:07

event density will theoretically be a constant function. For the moon this zenith angle corresponds with about 83°. For the sun this zenith angle is 70°. In this research the effect of implementing a cut-off at these zeniths is not studied. In a follow-up study it could be determined whether this impacts the event densities.

Chapter 5

Conclusion

In this study there are several topics that have been researched. The first topic is the influence of mispointing on a telescope. With mispointing an observed object will not only show up somewhere else than expected, the measurement itself will be distorted and blurred. The three parameters that characterize the mispointing (section 2.2) all have a different effect on a final measurement, see section 3.1.1.

The second topic is the analysis for the background signal for the moon as detected by the ORCA4 detector. This analysis shows that the ORCA4 can not determine a significantly constant average number of events in the background of the moon. In off-target measurements of the total number of entries in the neighbourhood of the source a deviation of the 5.38σ when no quality cuts were applied was found, figure 4.5. This is expected to be caused by systematic errors in the correction error for the event densities. This causes that the deficit of events around the moon could not be determined. It is shown that the data of the off-target measurements for the moon is more consistent with any flat line fit than its is with an average background (figure 4.7). A possible follow-up research is to find the systematic error in the correction factor. If this is found the methods of this research allow the evaluation of the background event density (section 4.2.2).

The same methods are used for the analysis of the background signal of the sun is carried out. In this analysis it is also found that the ORCA4 can not determine a significantly constant average number of events in the background of the sun. Here a deviance of 7.01σ is found in the total number of events around the off-target source, figure 4.9 (section 4.2.2).

The last topic of this study is concerning the increasing number of events per square degree as function of the distance to the sun. For the

sun it is found that the data of the off-target measurements of the sun is more consistent with a linearly increasing background than with an average background (figure 4.16). With a linear fit on the data of the off-target measurements of the sun an increase on the number of events per square degree of 2.77 ± 0.6 per degree is found. For the moon a similar analysis on the increase of the number of events per square degree finds 0.81 events per square degree per degree (section 4.3). This linearity is caused by the zenith angle coverage by the sun and moon. A future study is suggested where zenith angle cuts on the data are used to decrease this effect (section 4.3.3).

5.1 Acknowledgements

I would like to thank Dorothea Samtleben for the supervision of my project. As well I would like to thank the entire team of KM3NeT that is stationed at the Nikhef center in Amsterdam. The last person I would like to acknowledge is Clancy James for providing his code for the position tracking of the moon and the sun.

Bibliography

[1] M. Boden, *Time calibration and detector consistency cross checks of the KM3NeT detector using atmospheric particles*, Leiden University Repository (2019).

[2] S. Adrián-Martínez et al., *Letter of intent for KM3NeT 2.0*, Journal of Physics G Nuclear Physics **43**, 084001 (2016).

[3] F.W.Stecker and M.H.Salamon, *High Energy Neutrinos from Quasars*, 1995.

[4] B. Povh, K. Rith, C. Scholz, and F. Zetsche, *Particles and Nuclei*, Spring, 2014.

[5] A. Tatum.

[6] M. Sanguineti and C. Distefano, *Moon shadow observation with ANTARES and KM3NeT neutrino telescope*, EPJ Web of Conferences **116**, 06004 (2016).

[7] M. Aartsen, R. Abbasi, Y. Abdou, M. Ackermann, J. Adams, J. A. Aguilar SÃ¡nchez, M. Ahlers, D. Altmann, J. Auffenberg, X. Bai, M. Baker, S. Barwick, V. Baum, R. Bay, J. Beatty, S. Bechet, J. Tjus, K.-H. Becker, M. Bell, and M. Zoll, *Observation of the cosmic-ray shadow of the Moon with IceCube*, Physical Review D **89**, 102004 (2014).

[8] S. R. Majewski, *Celestial Coordinates*, 2020.

[9] P. Osborne, *The Mercator Projections*, Zenodo, 2013.

[10] D. R. Strebe, *Wikipedia*, 2011.

[11] D. R. Strebe, *Wikipedia*, 2011.

[12] Jhmadden, *Wikipedia*, 2015.

[13] B. Ó Fearraigh, *Track Reconstruction in KM3NeT*, KM3Net internal (2020).

[14] P. T. Wallace, *SLALIB Positional Astronomy Library*, 2005.

[15] *private communication Clancy James*.

[16] F. Bijma, M. Jonker, and A. van der Vaart, *Inleiding in de Statistiek*, Epsilon Uitgaven, 2018.

[17] *private communication Daniel Guderian*.

Chapter 6

Appendix

6.1 Code for simulation of mispointing

Below is the pseudo-code for simulating the mispointing. I left out the specifics for the customary functions. The reason for this is to keep it simple and understandable.

Specify certain time period and time steps
for *Every time step* **do**
    Calculate the real position of the moon
    Calculate the expected position of the moon (mispointed)
    Fill a grid with the difference of these positions
end

6.2 Plots

In this section you can find plots that are referenced in the thesis but were to redundant to plot in the actual text. This is mostly different quality cuts.

6.2.1 General Plots

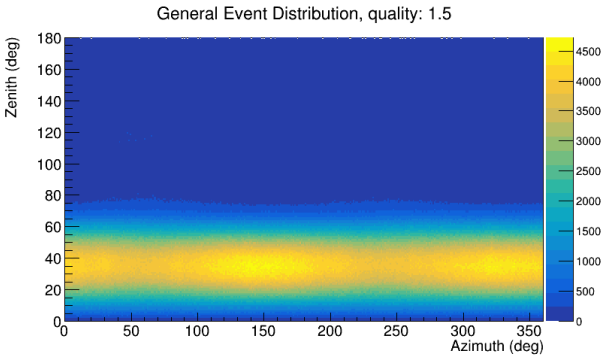

Figure 6.1: *The event distribution for the zenith and azimuth for the specified time, quality cut : 1.5. The binning is 360 by 180*

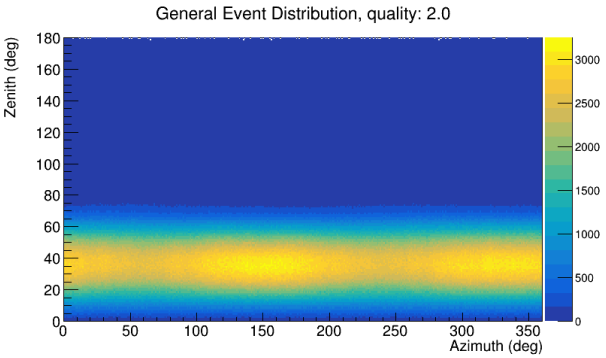

Figure 6.2: *The event distribution for the zenith and azimuth for the specified time, quality cut : 2.0. The binning is 360 by 180*

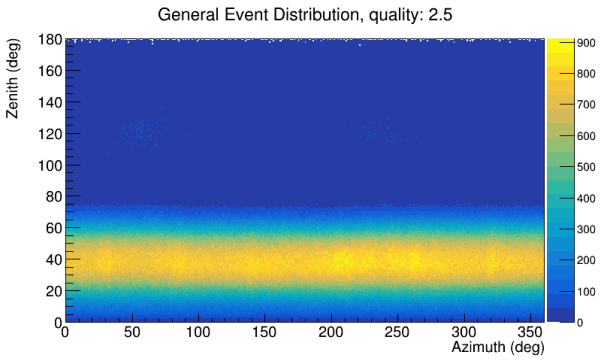

Figure 6.3: *The event distribution for the zenith and azimuth for the specified time, quality cut : 2.5. The binning is 360 by 180*

6.2.2 1D-Plots

Plots for the normalized event distributions.

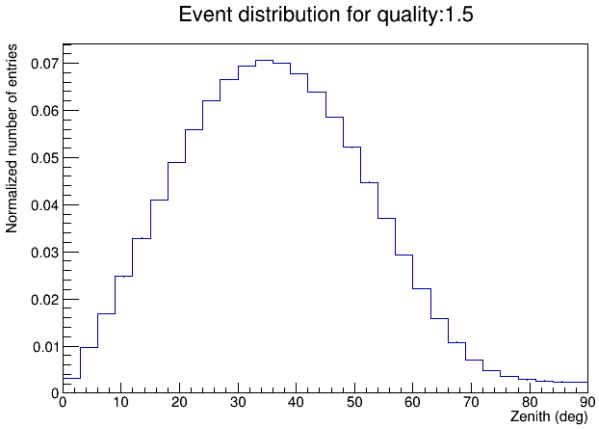

Figure 6.4: *The event normalized event distribution for each zenith smaller than 90°, quality: 1.5*

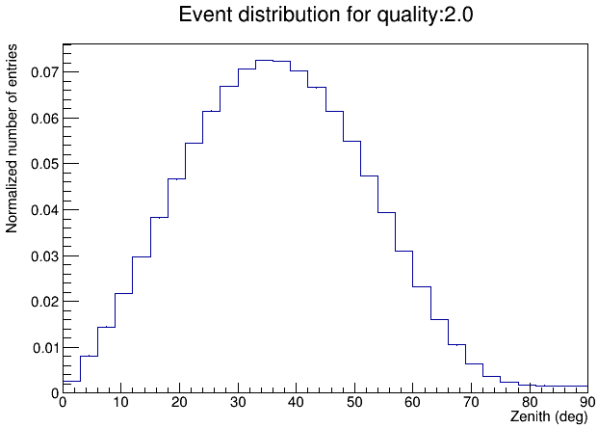

Figure 6.5: *The event normalized event distribution for each zenith smaller than 90°, quality: 2.0*

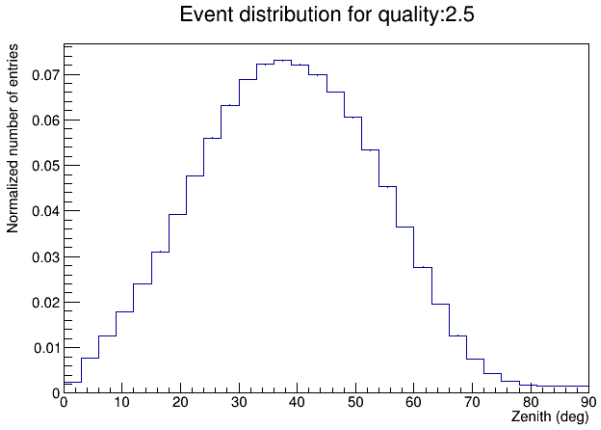

Figure 6.6: *The event normalized event distribution for each zenith smaller than 90°, quality: 2.5*

Plots for the chi^2 probabilities of the moon.

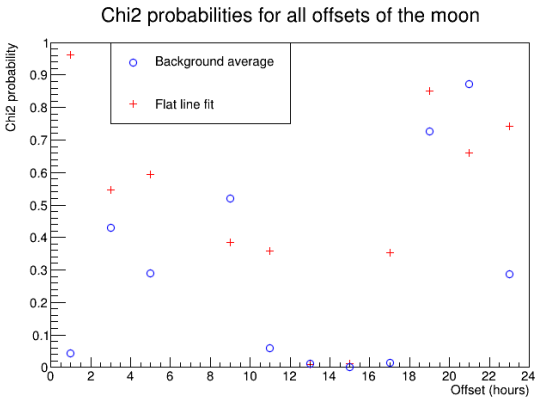

Figure 6.7: *The χ^2 probabilities of the data for all the offsets of the moon compared to the average background and to the fitted background, quality: 1.5*

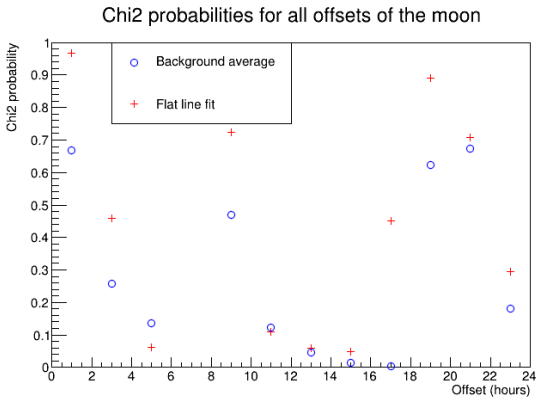

Figure 6.8: *The χ^2 probabilities of the data for all the offsets of the moon compared to the average background and to the fitted background, quality: 2.0*

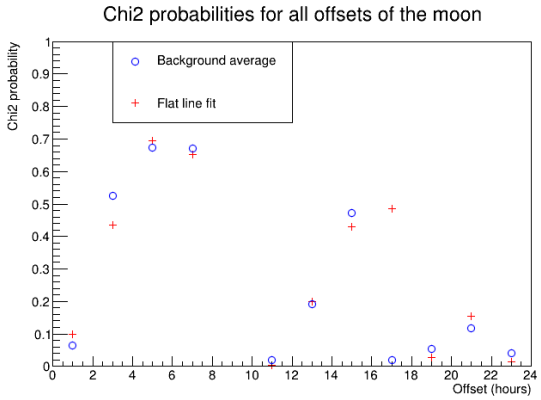

Figure 6.9: *The χ^2 probabilities of the data for all the offsets of the moon compared to the average background and to the fitted background, quality: 2.5*

Plots for the different quality cuts when looking at the moon

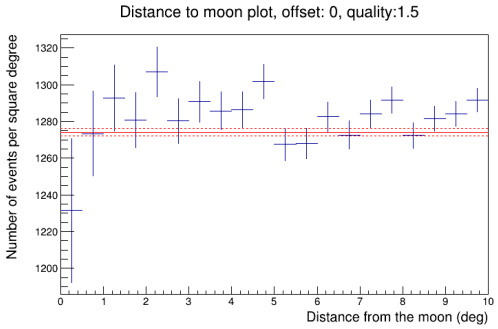

Figure 6.10: *The number of events per square degree as function of the distance to the moon. A quality cut of 1.5 is applied. The red line indicates the average background of off-source measurements. The dotted lines is* 1σ *interval.*

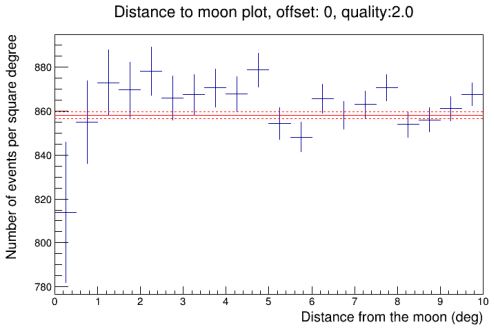

Figure 6.11: *The number of events per square degree as function of the distance to the moon. A quality cut of 2.0 is applied. The red line indicates the average background of off-source measurements. The dotted lines is* 1σ *interval.*

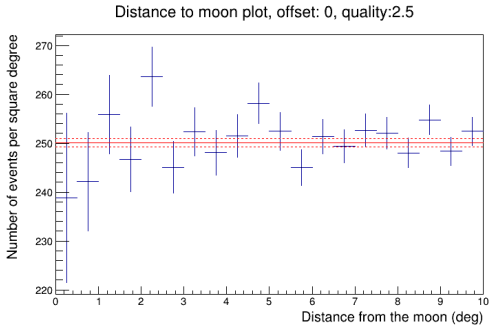

Figure 6.12: *The number of events per square degree as function of the distance to the moon. A quality cut of 2.5 is applied. The red line indicates the average background of off-source measurements. The dotted lines is* 1σ *interval.*

Plots for the chi^2 probabilities of the sun.

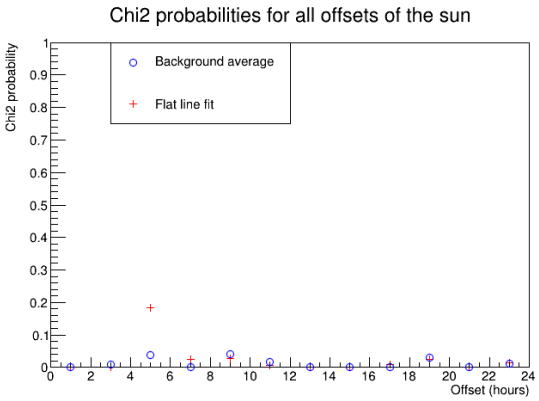

Figure 6.13: *The χ^2 probabilities of the data for all the offsets of the sun compared to the average background and to the fitted background, quality: 1.5*

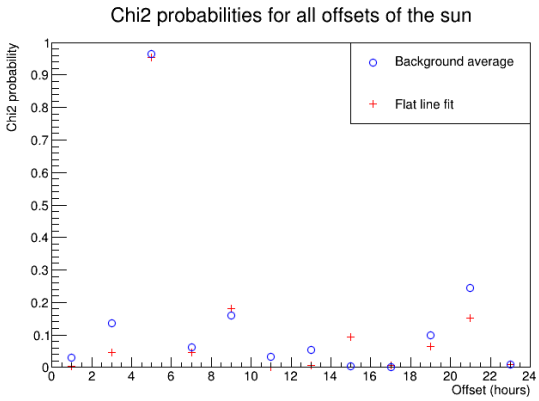

Figure 6.14: *The χ^2 probabilities of the data for all the offsets of the sun compared to the average background and to the fitted background, quality: 2.0*

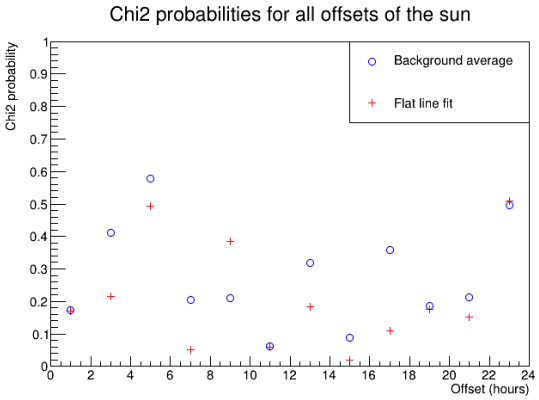

Figure 6.15: *The χ^2 probabilities of the data for all the offsets of the sun compared to the average background and to the fitted background, quality: 2.5*

Version of June 22, 2020– Created June 22, 2020 - 15:07

Plots for the different quality cuts when looking at the sun

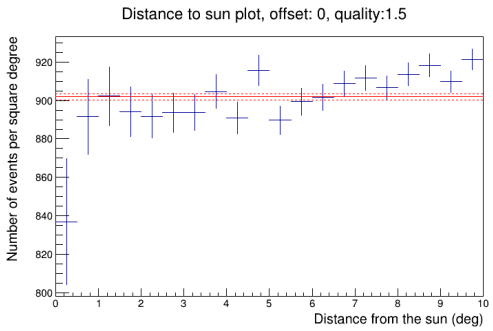

Figure 6.16: *The number of events per square degree as function of the distance to the sun. A quality cut of 1.5 is applied. The red line indicates the average background of off-source measurements. The dotted lines is* 1σ *interval.*

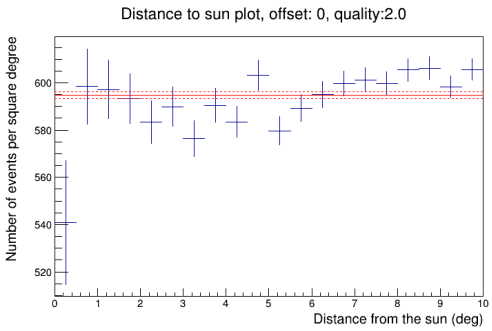

Figure 6.17: *The number of events per square degree as function of the distance to the sun. A quality cut of 2.0 is applied. The red line indicates the average background of off-source measurements. The dotted lines is* 1σ *interval.*

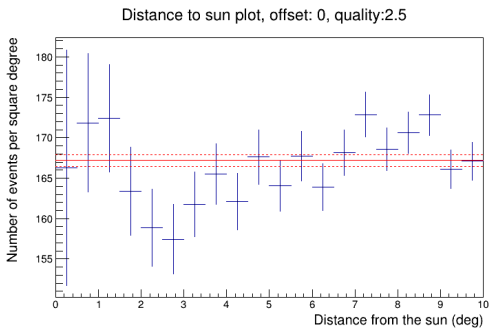

Figure 6.18: *The number of events per square degree as function of the distance to the sun. A quality cut of 2.5 is applied. The red line indicates the average background of off-source measurements. The dotted lines is* 1σ *interval.*

Plots for the *chi*^{2} probabilities of the sun when using a linear regression model.

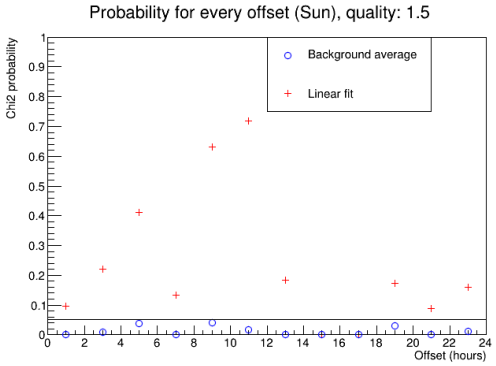

Figure 6.19: *χ^2 probabilities of the off-target data of the sun when compared to an average background and a linear average with slope 2.20 and intercept 888.47, quality: 1.5*

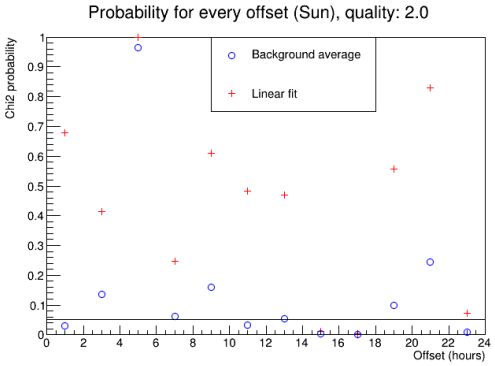

Figure 6.20: *χ^2 probabilities of the off-target data of the sun when compared to an average background and a linear average with slope 1.38 and intercept 586.33, quality: 2.0*

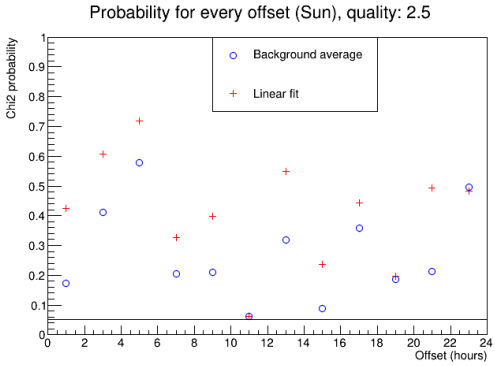

Figure 6.21: *χ^2 probabilities of the off-target data of the sun when compared to an average background and a linear average with slope 0.65 and intercept 165.23, quality: 2.5*

Plots for the chi^2 probabilities of the moon when using a linear regression model.

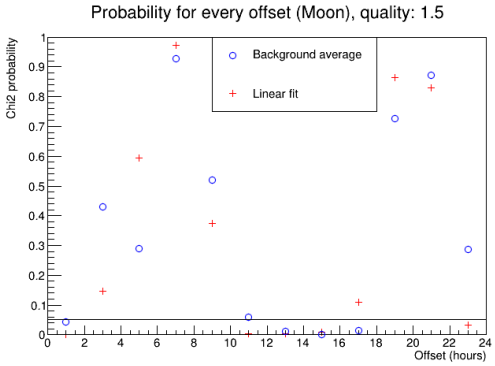

Figure 6.22: *χ^2 probabilities of the off-target data of the moon when compared to an average background and a linear average with slope 0.32 and intercept 1269.45, quality: 1.5*

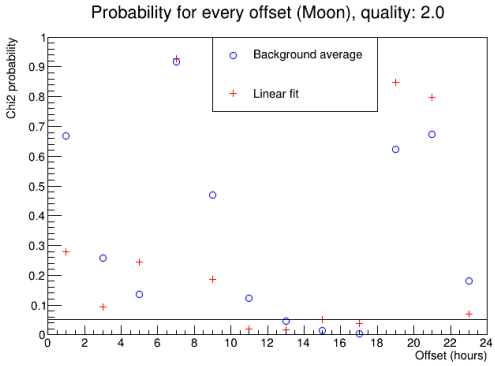

Figure 6.23: *χ^2 probabilities of the off-target data of the moon when compared to an average background and a linear average with slope -0.07 and intercept 856.81, quality: 2.0*

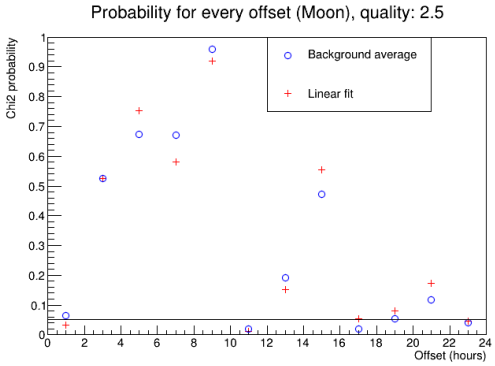

Figure 6.24: *χ^2 probabilities of the off-target data of the moon when compared to an average background and a linear average with slope -0.06 and intercept 250.12, quality: 2.5*

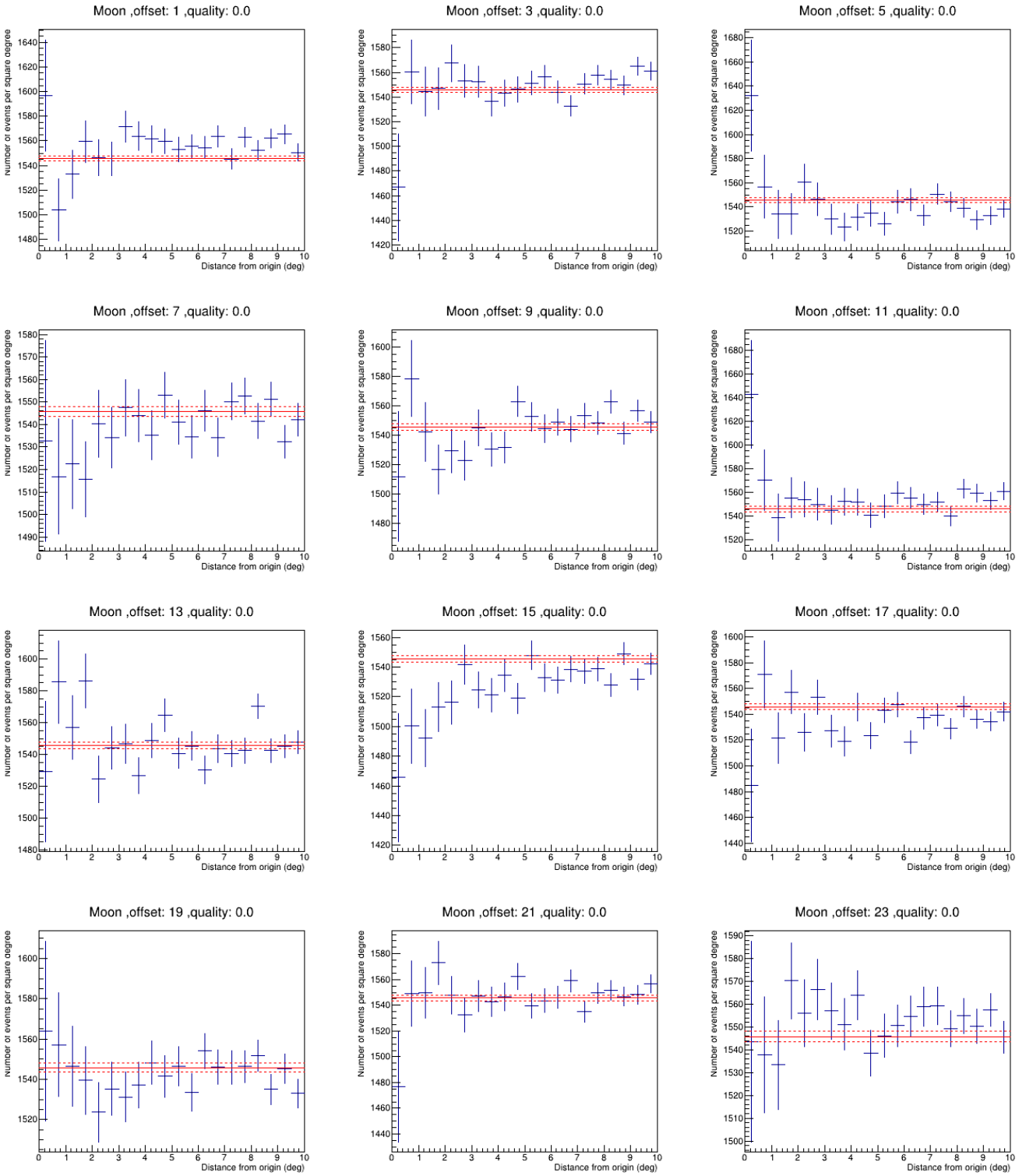

Figure 6.25: *Plots for the off-target sources of the moon, Quality: 0.0*

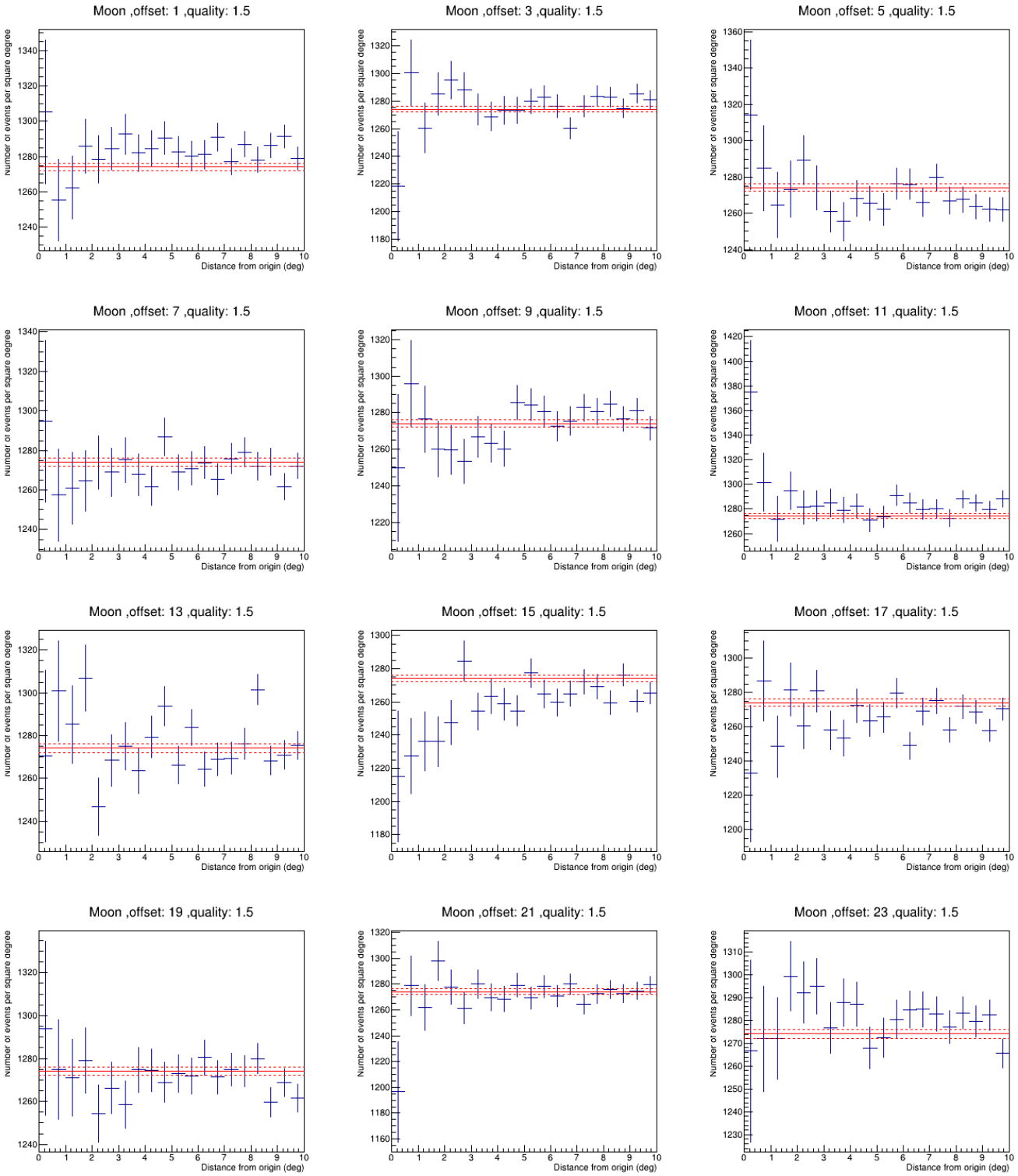

Figure 6.26: *Plots for the off-target sources of the moon, Quality: 1.5*

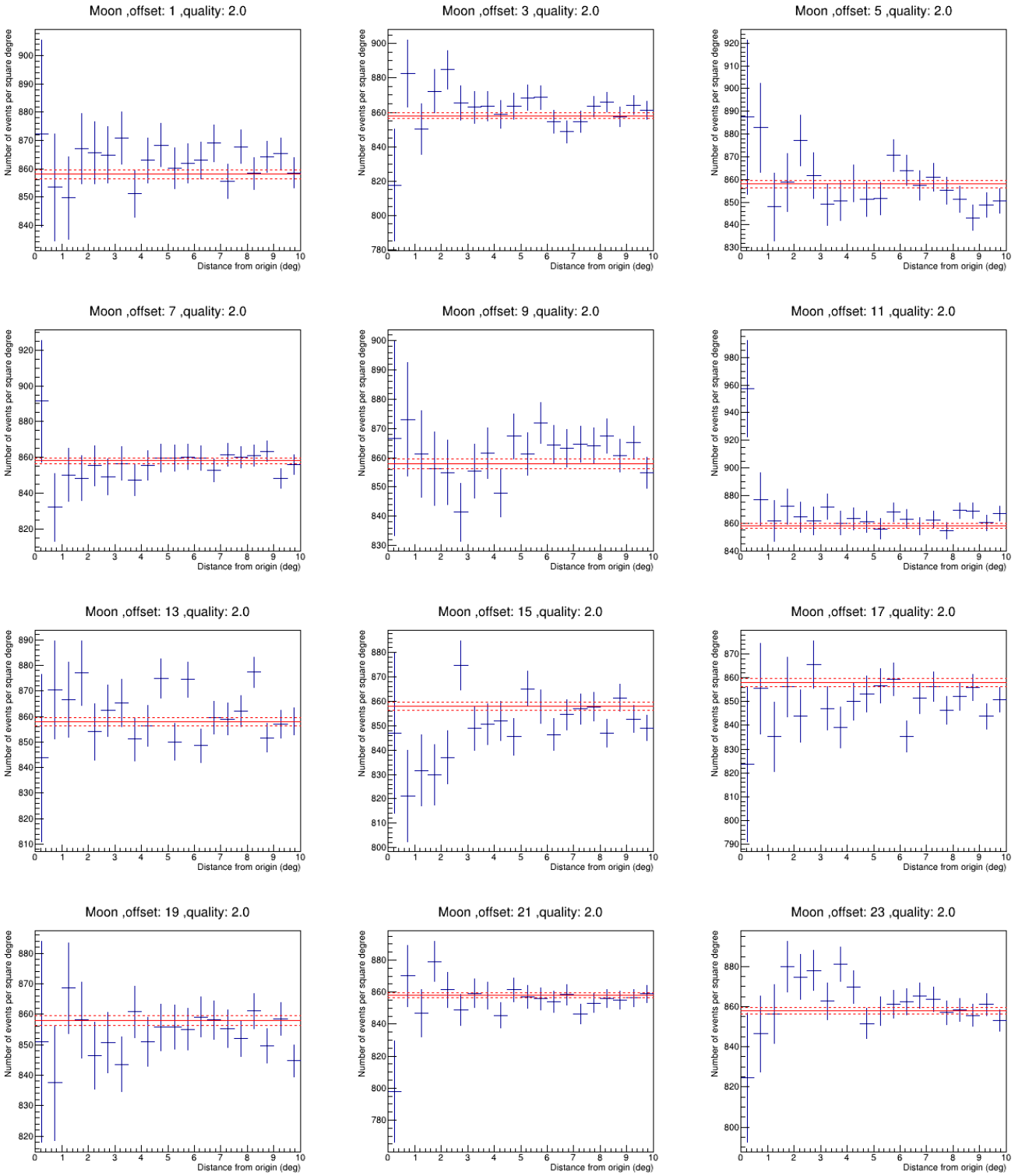

Figure 6.27: *Plots for the off-target sources of the moon, Quality: 2.0*

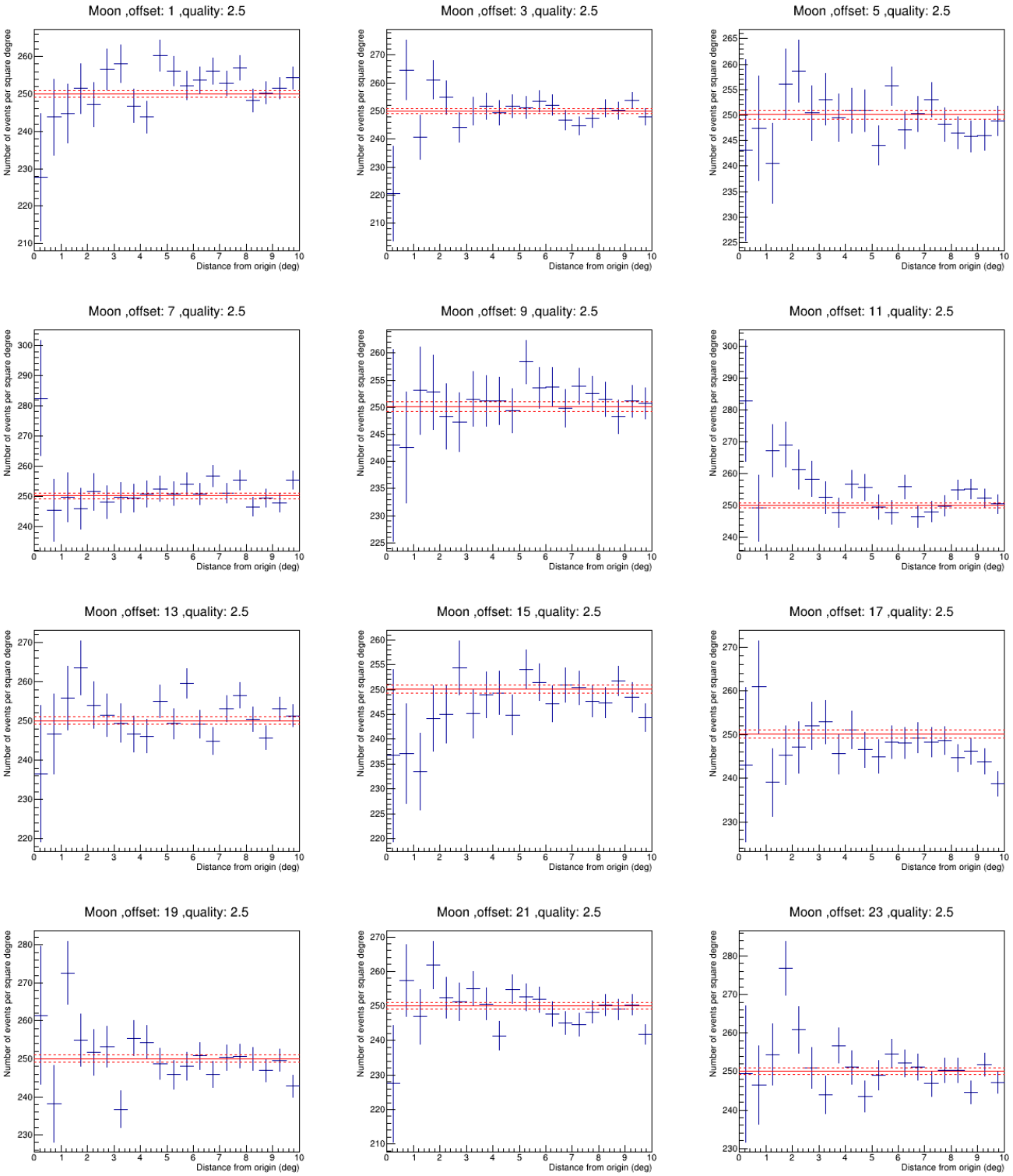

Figure 6.28: *Plots for the off-target sources of the moon, Quality: 2.5*

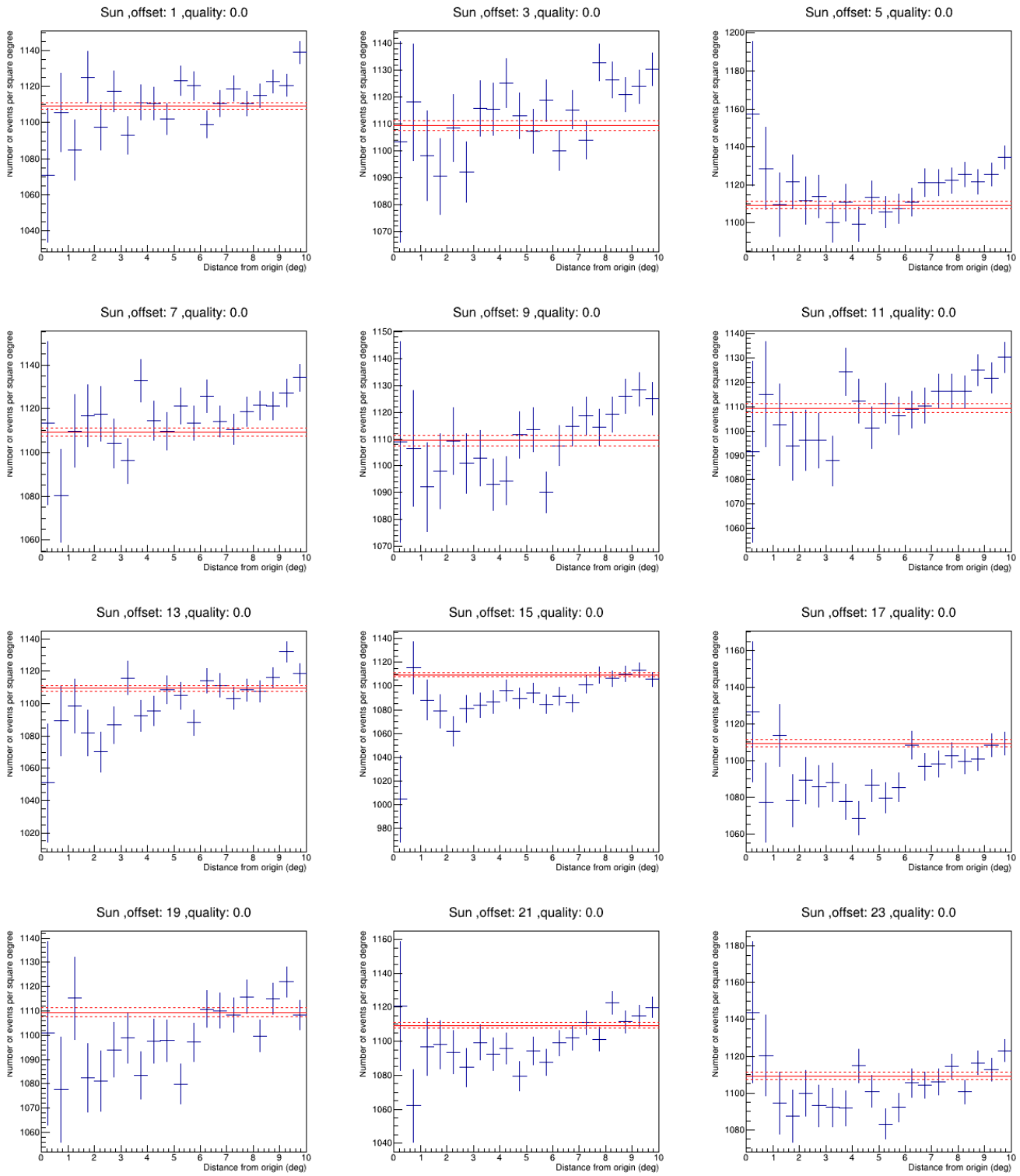

Figure 6.29: *Plots for the off-target sources of the sun, Quality: 0.0*

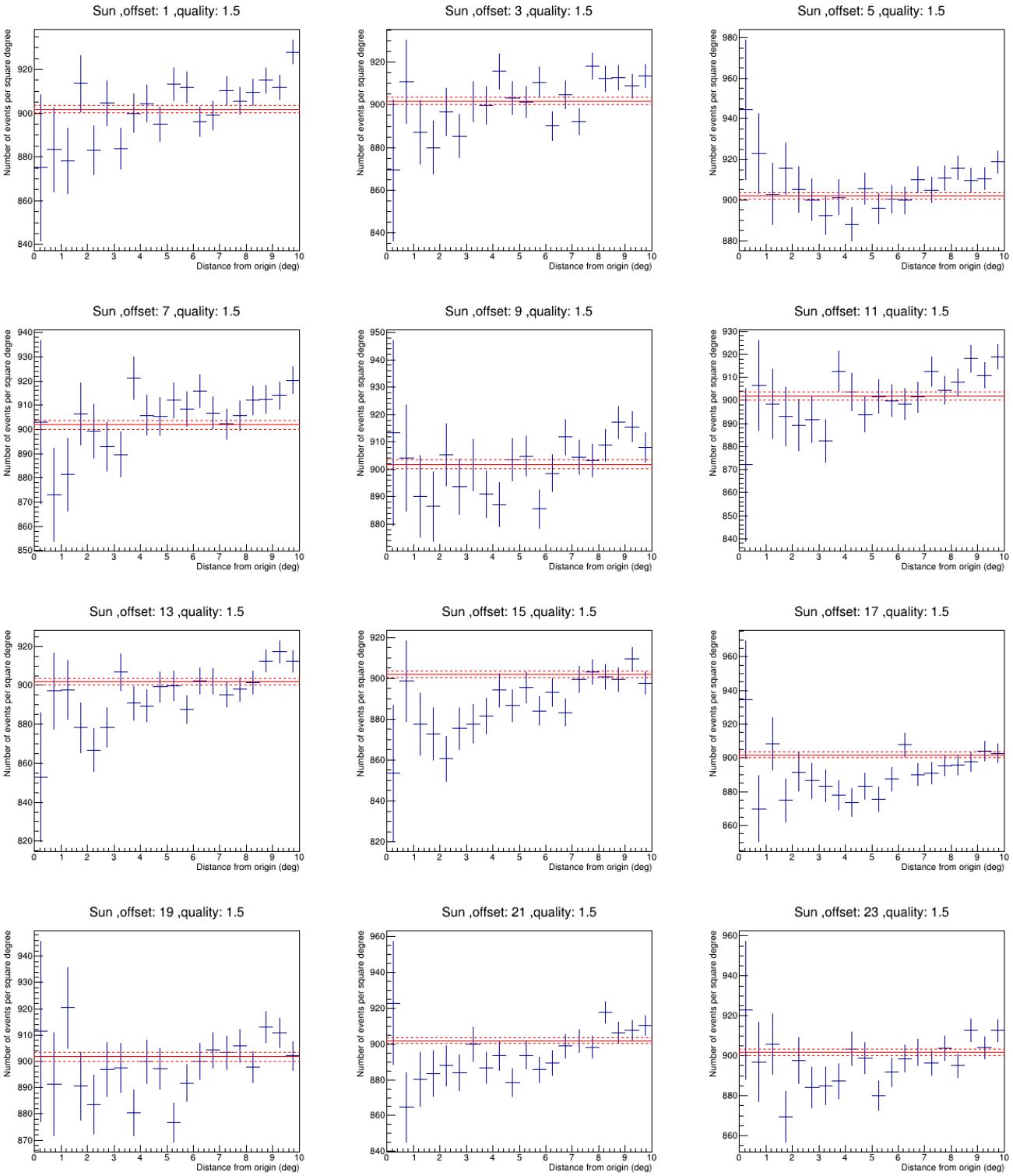

Figure 6.30: *Plots for the off-target sources of the sun, Quality: 1.5*

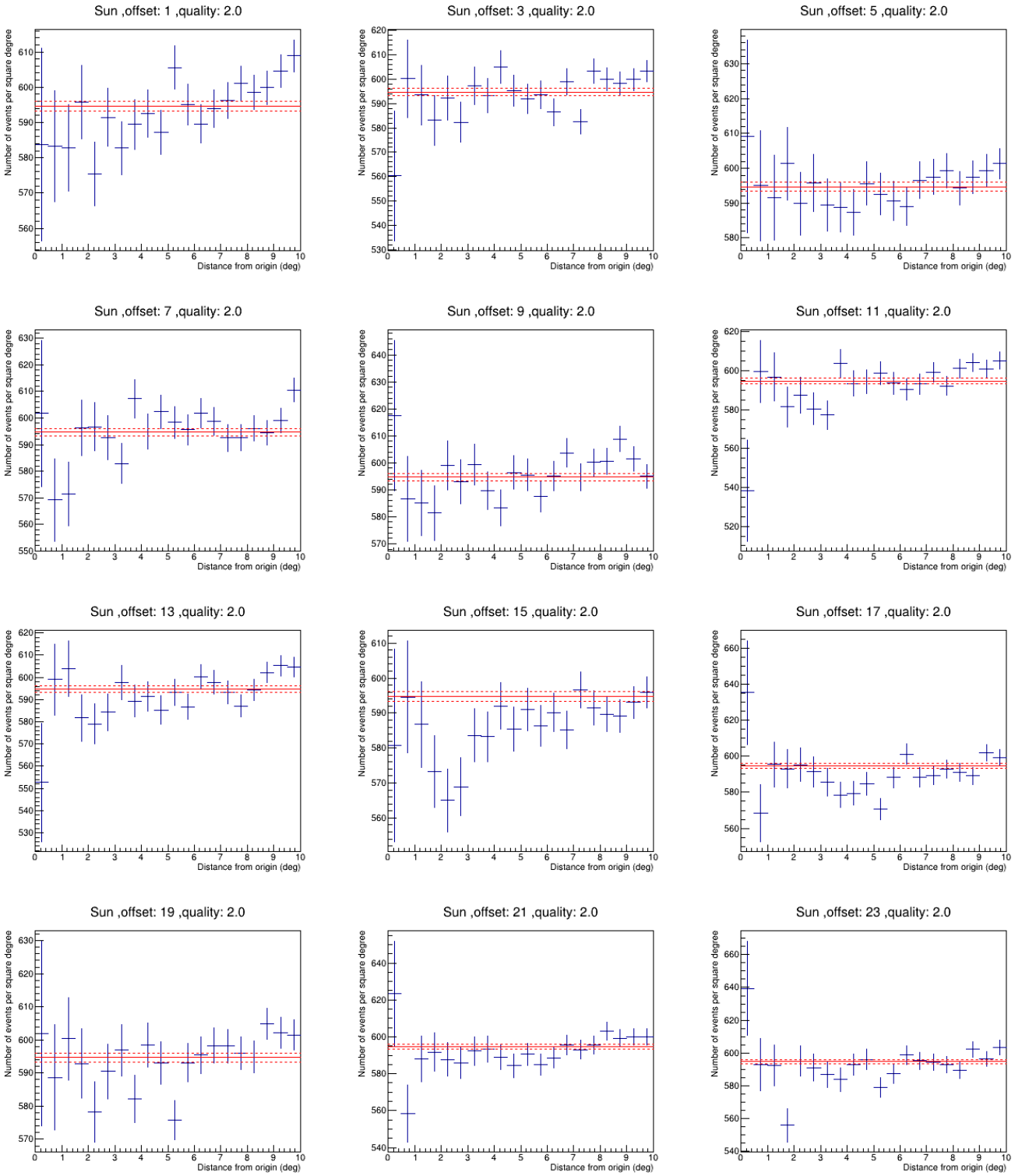

Figure 6.31: *Plots for the off-target sources of the sun, Quality: 2.0*

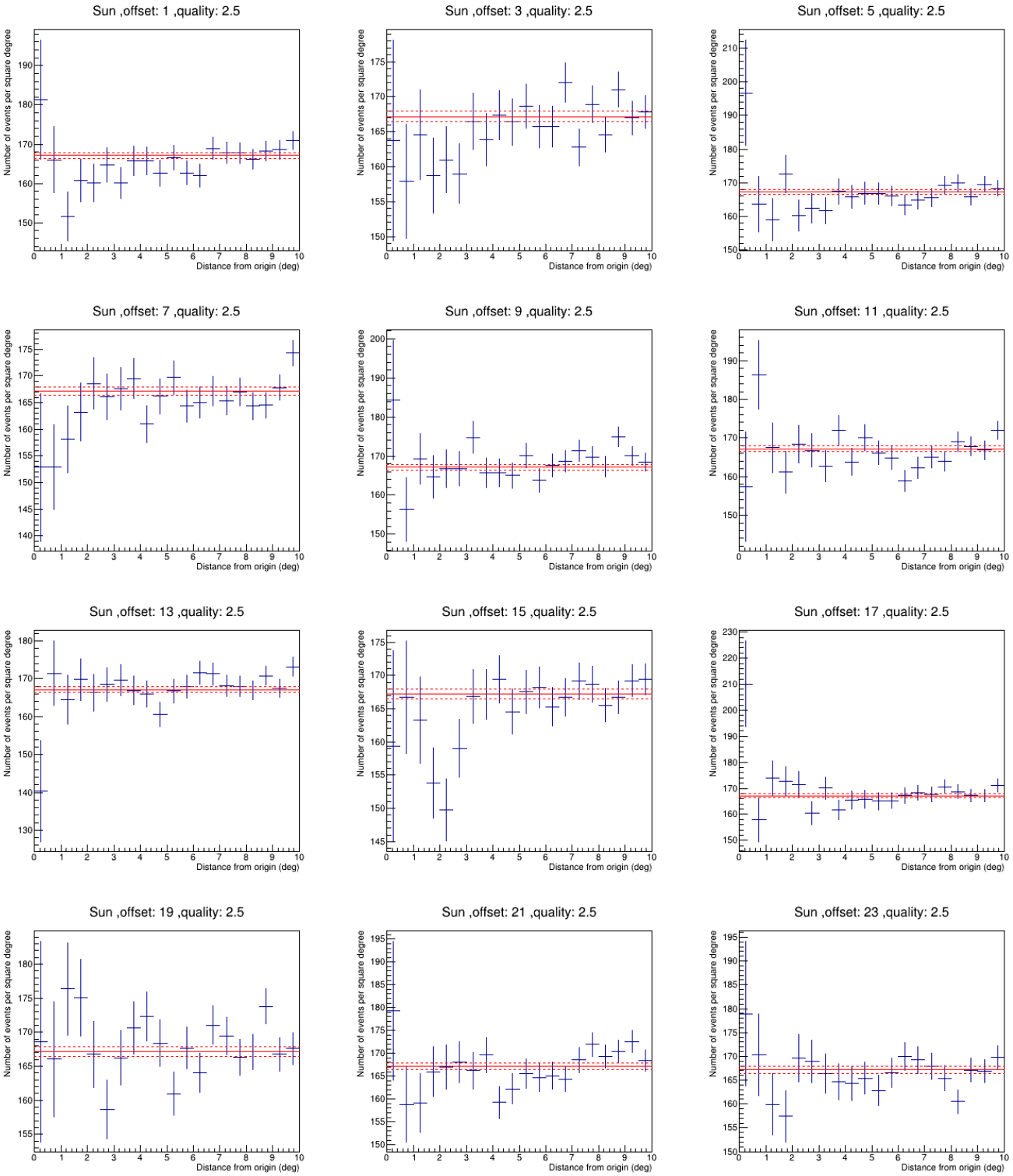

Figure 6.32: *Plots for the off-target sources of the sun, Quality: 2.5*